THE ASTRONOMICAL JOURNAL, 121:1936–1951, 2001 April

DYNAMICAL FAMILY PROPERTIES AND DARK HALO SCALING RELATIONS OF GIANT ELLIPTICAL GALAXIES

ORTWIN GERHARD AND ANDI KRONAWITTER
Astronomisches Institut, Universität Basel, Venusstrasse 7, CH-4102 Binningen, Switzerland; gerhard@astro.unibas.ch, krona@astro.unibas.ch

AND

R. P. SAGLIA AND RALF BENDER
Institut für Astronomie und Astrophysik, Scheinerstraße 1, D-81679 Munich, Germany; saglia@usm.uni-muenchen.de, bender@usm.uni-muenchen.de
Received 2000 June 9; accepted 2000 December 12

ABSTRACT

Based on a uniform dynamical analysis of the line-profile shapes of 21 mostly luminous, slowly rotating, and nearly round elliptical galaxies, we have investigated the dynamical family relations and dark halo properties of ellipticals. Our results include: (i) The circular velocity curves (CVCs) of elliptical galaxies are flat to within $\simeq 10\%$ for $R \gtrsim 0.2R_e$. (ii) Most ellipticals are moderately radially anisotropic; their dynamical structure is surprisingly uniform. (iii) Elliptical galaxies follow a Tully-Fisher (TF) relation with marginally shallower slope than spiral galaxies, and $v_c^{\max} \simeq 300$ km s^{-1} for an L_B^* galaxy. At given circular velocity, they are ~ 1 mag fainter in B and ~ 0.6 mag in R and appear to have slightly lower baryonic mass than spirals, even for the maximum M/L_B allowed by the kinematics. (iv) The luminosity dependence of M/L_B indicated by the tilt of the fundamental plane (FP) is confirmed. The tilt of the FP is not caused by dynamical or photometric nonhomology, although the latter might influence the slope of M/L versus L. It can also not be due only to an increasing dark matter fraction with L for the range of IMF currently discussed. It is, however, consistent with stellar population models based on published metallicities and ages. The main driver is therefore probably metallicity, and a secondary population effect is needed to explain the K-band tilt. (v) These results make it likely that elliptical galaxies have nearly maximal M/L_B (minimal halos). (vi) Despite the uniformly flat CVCs, there is a spread in the luminous to dark matter ratio and in cumulative $M/L_B(r)$. Some galaxies have no indication for dark matter within $2R_e$, whereas for others we obtain local M/L_B-values of 20–30 at $2R_e$. (vii) In models with maximum stellar mass, the dark matter contributes $\sim 10\%$–40% of the mass within R_e. Equal interior mass of dark and luminous matter is predicted at ~ 2–$4R_e$. (viii) Even in these maximum stellar mass models, the halo core densities and phase-space densities are at least ~ 25 times larger and the halo core radii ~ 4 times smaller than in spiral galaxies of the same circular velocity. The increase in M/L sets in at ~ 10 times larger acceleration than in spirals. This could imply that elliptical galaxy halos collapsed at high redshifts or that some of the dark matter in ellipticals might be baryonic.

Key words: dark matter — galaxies: elliptical and lenticular, cD — galaxies: formation — galaxies: halos — galaxies: kinematics and dynamics — galaxies: stellar content

1. INTRODUCTION

Hierarchical theories of galaxy formation predict that elliptical galaxies should be surrounded by dark matter halos. The study of these halos has been difficult, however, because of the lack of suitable and easily interpreted tracers such as the H I rotation curves in spiral galaxies. Recent work in several fields, however, leaves no doubt about the existence of dark matter in ellipticals: X-ray data on their hot gas atmospheres imply that dark halos in ellipticals are ubiquitous and that the mass-to-light ratios are $M/L \sim 100$ on scales of ~ 100 kpc (Mushotzky et al. 1994; Matsushita et al. 1998; Loewenstein & White 1999). Gravitational lensing studies (Kochanek 1995; Keeton, Kochanek & Falco 1998; Griffiths et al. 1998) show evidence for large M/L in lens elliptical galaxies, and stellar-dynamical studies based on absorption line profile shapes have given strong constraints on the mass distributions to $\sim 2R_e$ (Rix et al. 1997; Gerhard et al. 1998; Saglia et al. 2000a), with a small to moderate dark matter fraction inside $2R_e$.

Despite of this progress, the detailed mass distributions in elliptical galaxies and their variations with luminosity remain largely unknown. Has the luminous matter segregated dissipatively in the halo potential? Is there a "conspiracy" between luminous and dark matter to produce a flat rotation curve, like in spiral galaxies? How do the mass-to-light ratio, the slope of the circular velocity curve, or the orbital anisotropy scale with luminosity? Is the tilt of the fundamental plane simply related to a variation of the dynamical M/L with L? Do elliptical galaxies follow a Tully-Fisher relation? How do the scale radii and densities of elliptical galaxy halos compare to those of spiral galaxies?

The purpose of this paper is to address some of these questions on the basis of a new dynamical study by Kronawitter et al. (2000, hereafter K+2000), who analyzed the dynamical structure and mass distribution for a sample of 21 bright elliptical galaxies. Continuing from previous work by our group (Gerhard et al. 1998; Saglia et al. 2000a), these authors modeled the line profile shapes of in total 17 E0/E1 and four E2 galaxies for which kinematic data including line profile information were available from their own observations or from the literature. The dynamical structure of these galaxies turned out to be remarkably uniform. Most galaxies require moderate radial anisotropy in their main bodies (at $\sim 0.5R_e$). Their circular velocity curves are all consistent with being flat outside $\simeq 0.2R_e$. The M/L ratio

profiles begin to rise at around 0.5–2R_e and are consistent with X-ray and other data where available, although from the kinematic data alone constant M/L models can only be ruled out at 95% confidence in a few galaxies.

This sample provides a new and much improved basis for investigating the dynamical family properties of elliptical galaxies, which is the subject of the present study. In § 2, we analyze the unexpectedly uniform dynamical structure of these elliptical galaxies. In § 3, we investigate the dependence on luminosity, discussing the Faber-Jackson, Tully-Fisher, and fundamental plane relations. In § 4, we relate the dynamical mass-to-light ratios to the stellar population properties. In § 5 we discuss the structure of the dark halos of these ellipticals. Our conclusions are summarized in § 6.

2. DYNAMICAL STRUCTURE

The elliptical galaxies analyzed by K + 2000 divide in two subsamples, one with new extended kinematic data, reaching typically to $\sim 2R_e$ ("EK sample," the data are from Kronawitter et al. and from several other sources referenced there), and one with older and less extended kinematic measurements ("BSG sample"; this is a subsample from Bender, Saglia & Gerhard 1994). Based on these data and mostly published photometry, K + 2000 constructed non-parametric spherical models from which circular velocity curves, radial profiles of mass-to-light ratio, and anisotropy profiles for these galaxies were derived, including confidence ranges.

The galaxies were selected to rotate slowly if at all and to be as round as possible on the sky. They are luminous elliptical galaxies ($M_B \simeq -21 \pm 2$).[1] The expected mean intrinsic short-to-long axis ratio for such a sample of luminous ellipticals is $\langle c/a \rangle = 0.79$. The mean systematic effects arising from the use of spherical models and the possible presence of small embedded face-on disks are small for the sample as a whole, but may be non-negligible in individual cases (see K + 2000, § 5.1).

2.1. *Circular Velocity Curves*

Circular velocity curves (CVCs) for all galaxies in the sample are shown in Figure 1, in three bins roughly ordered by luminosity. CVCs normalized by the respective maximum circular velocity are shown in Figure 2 separately for the two subsamples. The plotted curves correspond to the "best" models of K + 2000, which are taken from the central region of their 95% confidence interval for each galaxy, respectively. Based on dynamical models near the boundaries of the confidence interval, the typical uncertainty in the outermost circular velocity is ±10%–15%. The expected mean systematic error from flattening along the line of sight is smaller; cf. § 5.1 of K + 2000.

The most striking result from these diagrams is that at the ≃10% level all CVCs are flat outside $R/R_e \simeq 0.2$. This result is most significant for the galaxies with the extended data, while for many galaxies from the BSG sample the radial extent of the data is insufficient to show clear trends. However, in cases where X-ray data are available (NGC 4472, 4486, 4636) the mass profiles of the "best" models approximately match those from the X-ray analysis even for those galaxies (see K + 2000).

[1] Throughout this paper we use a Hubble constant $H_0 = 65$ km s^{-1} Mpc^{-1} unless explicitly noted otherwise.

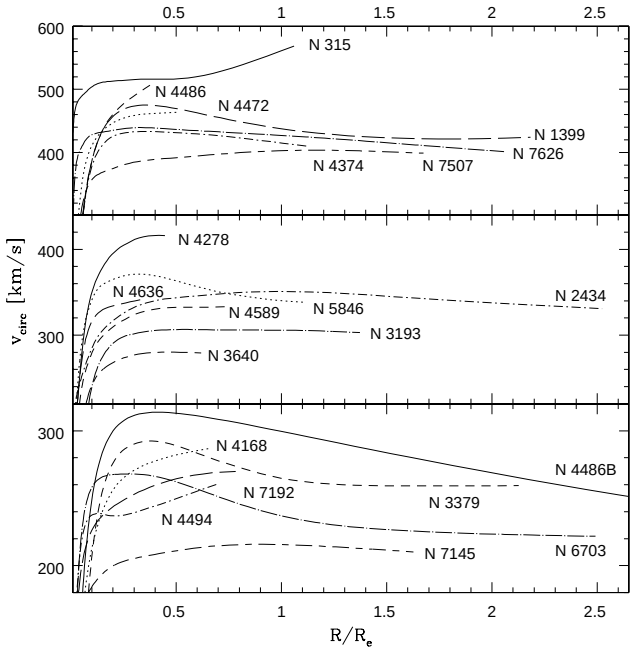

FIG. 1.—The "best model" circular velocity curves of all galaxies from the K + 2000 sample plotted as a function of radius scaled by the effective radius R_e. The panels are roughly ordered by luminosity.

This result is illustrated further by Figure 3, which shows the derived ratio $v_c(R_{max})/v_c^{max}$ for all galaxies of the EK-sample. Here $v_c(R_{max})$ is the circular velocity at the radius of the last kinematic data point, and v_c^{max} is the maximum circular velocity in the respective "best" model. For NGC 315 $v_c(0.6R_e)$ was used instead of v_c^{max}. The error bars plotted correspond to the 95% confidence range for $v_c(R_{max})$, compared to which the uncertainty in v_c^{max} can be

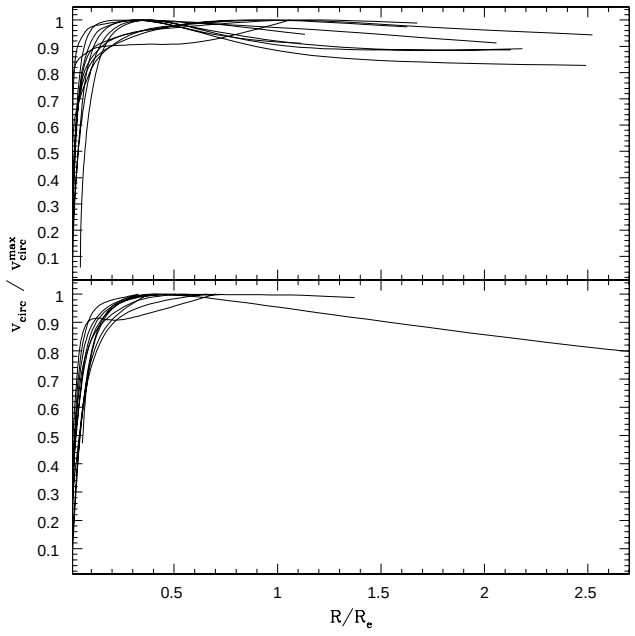

FIG. 2.—Same circular velocity curves, normalized by the maximum circular velocity. The upper panel now shows the galaxies from the EK subsample of K + 2000, the lower panel those from the BSG subsample. The extended curve in the lower panel is for the compact elliptical NGC 4486B.

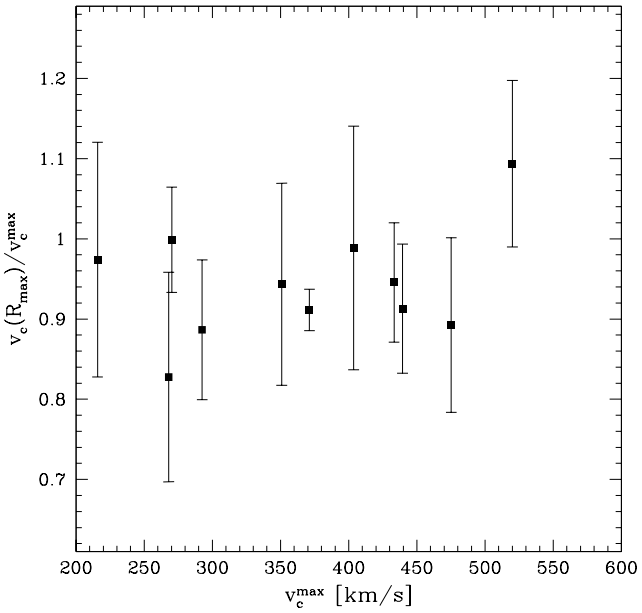

FIG. 3.—The ratio $v_c(R_{max})/v_c^{max}$ for all galaxies from the EK-sample, showing the gradient in the circular velocity curves. The error bars plotted correspond to the range of $v_c(R_{max})$ from the 95% confidence models of K + 2000.

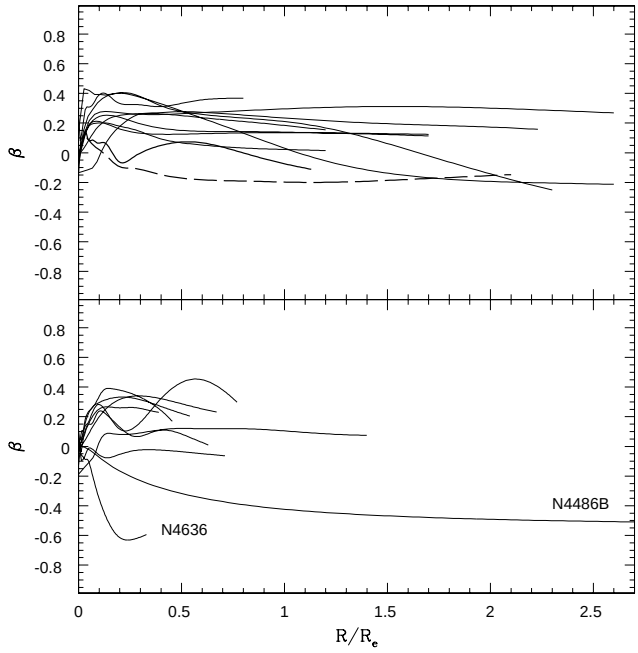

FIG. 4.—Velocity anisotropy β as a function of radius: (*top*) for the galaxies with extended data (EK subsample), (*bottom*) for the galaxies from the BSG subsample.

neglected. Most of these galaxies have $v_c(R_{max})/v_c^{max} \simeq 0.9$–1.0 with a median at 0.94, and 95% confidence ranges $\sim \pm 0.1$.

The galaxies in the EK sample appear to show a "bimodal" distribution of CVC shapes in Figures 1 and 2: For one group of galaxies the "best" model CVC has a peak near $0.3R_e$ and then falls slightly until it becomes flat at $\simeq 1R_e$ (NGC 1399, NGC 3379, NGC 5846, and NGC 6703, the latter has the largest drop). In the other group the CVC rises rapidly until $\simeq 0.2R_e$ and reaches a peak at $\simeq 1R_e$ after which it remains nearly flat (NGC 2434, NGC 7145, NGC 7192, NGC 7507). NGC 4374 and NGC 7626 may be cases from the first group where the flat part is not yet seen in the data. The rise of the CVC of NGC 315 seen near R_{max} in Figure 1 may not be real; a flat CVC appears also consistent with the kinematic data (see discussion in K + 2000). The difference between these CVC shapes is about a $\simeq 2\,\sigma$ result when comparing the model confidence bands for EK galaxies of either type, but this estimate does not include possible systematic effects from the use of spherical models. If the differences in CVC shapes are real, they could reflect small variations in the degree of dissipation and mass segregation of the baryonic component during the formation process. In any case no clear trend with galaxy luminosity is seen.

2.2. *Anisotropy*

Figure 4 shows the radial profiles of the anisotropy parameter $\beta = 1 - \sigma_t^2/\sigma_r^2$ for all galaxies. Here σ_r and σ_t are the intrinsic radial and one-dimensional tangential velocity dispersions, and $\beta = 1,\ 0,\ -\infty$ for completely radial, isotropic, and circular orbit distributions, respectively. Because it is a deprojected quantity, the anisotropy derived from our models is considerably more uncertain than the total mass $M(r)$; see Gerhard et al. (1998) for further discussion. The uncertainties are particularly large near the outer boundary of the data, where the range of β-values in models corresponding to the allowed potentials is usually 0.2–0.5. For the inner profiles, the allowed range is typically 0.1–0.2, sometimes 0.3. Nonetheless, Figure 4 shows a clear trend in that almost all galaxies are radially anisotropic in the inner (best-constrained) regions, with the peak of the anisotropy often near 0.2 R_e with values of $\beta = 0.2 \ldots 0.4$. There are two cases in the EK sample which are exceptional in that they are consistent with isotropy over the whole radial range. These two are NGC 315 (*thick solid line*), a cD galaxy, and NGC 7626 (*thick long-dashed line*), which is classified as E pec. Despite their less extended and lower S/N data, the galaxies from the BSG sample show a similar trend, again with two exceptions: NGC 4636, which we do not consider a very reliable case, and NGC 4486B, which is exceptional in almost all respects.

To get a more robust estimate of the anisotropy we have averaged the anisotropy profile between 0.1 R_e and $\min(R_e, R_{max})$, where R_{max} is the radius of the outermost kinematic data point. These averaged anisotropies are plotted in Figure 5 versus the maximum circular velocity from Figure 1. In a few cases this is the circular velocity at the outer boundary of the modeled range. Most galaxies with extended data show a clear maximum of the CVC whereas the BSG galaxies have CVCs which may still rise outward. For these the true maximum probably lies outside the range of the kinematic data. The error bars plotted for β show the standard deviation from the mean over the radial range used in the averaging. The errors plotted for v_c are equal to $\pm 1/2$ the separation of the extreme models in the confidence interval, near the radius where the best model has its maximum. The figure shows again that all galaxies but two (NGC 4486B and NGC 4636) have a mean radial anisotropy in the range from $\beta \simeq 0$ to $\beta \simeq 0.35$, and also that there is no dependence on circular velocity (or luminosity).

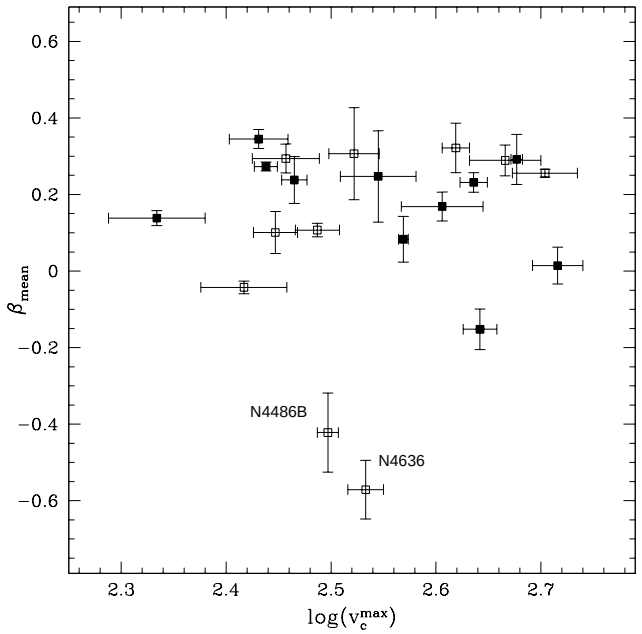

FIG. 5.—Average velocity anisotropy β, calculated over the range $0.1R_e$ to $1R_e$ or R_{max} if $R_{max} < R_e$, vs. maximum circular velocity. *Filled squares*: Galaxies with extended data, EK subsample. *Open squares*: Galaxies from BSG subsample; see text and K+2000. The error bars plotted for β show the standard deviation from the mean in the radial range used in the averaging.

Radial anisotropy has also been inferred from three-integral axisymmetric models for several flattened elliptical galaxies: NGC 1600 (E3.5, Matthias & Gerhard 1999), NGC 2300 (E2, Kaeppeli 1999), NGC 2320 (E3.5, Cretton, Rix, & de Zeeuw 2000, NGC 3379 (E1, Gebhardt et al. 2000). This makes it unlikely that our results are severely biased by the use of spherical dynamical models. As discussed in K+2000, the mean intrinsic short-to-long axis ratio for our sample of elliptical galaxies is $\langle c/a \rangle = 0.79$. Because these are luminous galaxies, rotation will not contribute substantially to any flattening, so except for the flattest galaxies the bias introduced by face-on circular orbits will be small. On the other hand, possibly embedded face-on disks are likely to be less than 0.1–$0.3R_e$ in size on statistical grounds (Mehlert et al. 1998). In three galaxies of our sample, such disks are known and extend to 6″, 7″, and 8″ in NGC 4472, NGC 4494, and NGC 7626, respectively. In these very inner regions, these disks might cause the anisotropy to be overestimated by $\simeq 0.2$, but they will not affect the globally averaged results significantly.

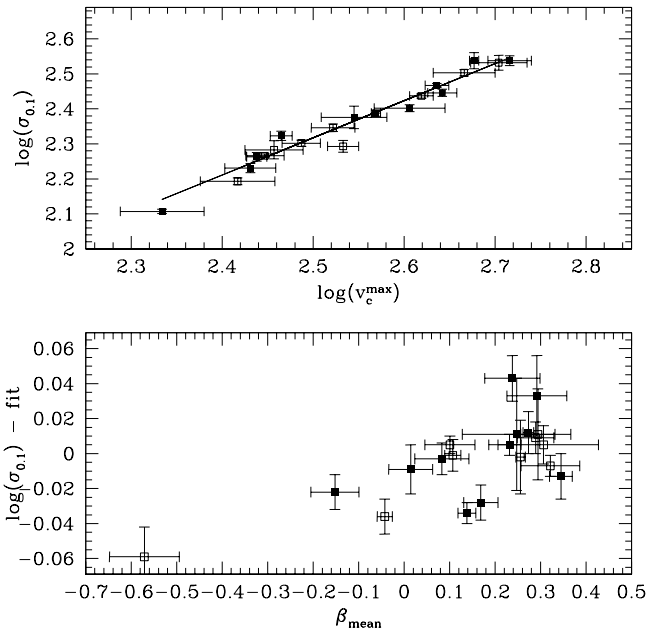

FIG. 6.—*Top*: The correlation between the averaged central velocity dispersion and the inferred maximum circular velocity. *Bottom*: The residuals from this correlation plotted vs. the mean orbital anisotropy defined in § 2.2. Symbols as in Fig. 5.

2.3. v_c^{max}–$\sigma_{0.1}$

We have found that both the circular velocity curves and the anisotropy profiles of elliptical galaxies are surprisingly similar. In zeroth order the CVCs can thus be characterized by two scaling constants, the effective radius and a velocity scale. In Figure 5 we have used the maximum circular velocity; but in fact it should not matter which velocity is used to set the scale. In particular, we would expect that a suitably defined central velocity dispersion could equally be used. A little care is needed, however, since the measured central velocity dispersion may be influenced by the gravitational field of a central black hole and by the resolution of the kinematic data. We therefore use an average central velocity dispersion $\sigma_{0.1}$, defined as the square root of the average of all measured $\sigma_i^2 \equiv \sigma^2(R_i)$ inside $0.1R_e$ or 3″, whichever is the larger of the two radii. This would be the inner luminosity-averaged rms velocity dispersion if the surface brightness profile were exactly proportional to R^{-1}.

Figure 6 shows a plot of $\sigma_{0.1}$ versus the maximum circular velocity for all elliptical galaxies in our sample but NGC 4486B. The error bars for v_c^{max} are taken from the allowed model range as before. For the error bars in the $\sigma_{0.1}$ we have taken the larger of

$$\frac{\Delta\sigma_{0.1}}{\sigma_{0.1}} = \frac{[\sum_i (\sigma_i^2 - \sigma_{0.1}^2)^2]^{1/2}}{2\sqrt{N-1}\,\sigma_{0.1}^2} \quad (1)$$

and a weighted observational error in $R \leq 0.1R_e$, $\Delta\sigma_{obs} \equiv (\sum_i \Delta\sigma_i^{-2})^{-1/2}$. For some galaxies the actual error of $\sigma_{0.1}$ may be smaller than this conservative estimate from the standard deviation of the σ_i^2, but we have used this because several galaxies have velocity dispersion gradients in the central $0.1R_e$. Figure 6 shows a very good correlation; the slope is 1.062 ± 0.058 for a reduced $\chi^2 = 0.87$, as determined by the routine "fitexy" of Press et al. (1992). This routine fits a straight line to the data points by minimizing a χ^2 function which involves the errors in both the x- and y-variables. Thus, the fitted relation is completely consistent with linear; explicitly,

$$\sigma_{0.1} = 0.66 v_c^{max} . \quad (2)$$

The lower panel of Figure 6 shows that the residuals from this relation are correlated with the mean orbital anisotropy defined in § 2.2 (the correlation would be somewhat stronger had we plotted it in terms of the maximum anisotropy). Differences in dynamical structure thus cause some scatter in the relation between $\sigma_{0.1}$ and v_c^{max} but their influence on

this and other global correlations is small. In this sense the dynamical structure of these ellipticals is indeed very uniform.

3. SCALING RELATIONS

3.1. *Faber-Jackson Relation*

The well-known relation between the total magnitude and central velocity dispersion for elliptical galaxies (Faber & Jackson 1976) is shown in the top panel of Figure 7 for the K+2000 sample of ellipticals, with $\sigma_{0.1}$ in place of the central dispersion. In this plot and all subsequent similar plots B_T^i is twice the total integrated B-band absolute magnitude within R_e (col. [7] of Table 4 in K+2000). The errors in these B_T^i magnitudes are set to 0.3 mag. This accounts for observational errors and uncertainties in the distances. The latter are estimated as approximately 0.25 mag from the intrinsic scatter of the Dn-σ relation, the depth of clusters (in case of group/cluster distances), and a comparison of various distance determinations by Tonry et al. (1997). The fitted slope of the Faber-Jackson relation for our ellipticals (again using the errors in both variables) is -4.89 ± 1.12, i.e., $L_B \propto (\sigma_{0.1})^{1.96\pm0.45}$. The fit excludes NGC 4486B; this galaxy is a close companion of M87 and its low luminosity for its high circular velocity suggests that the galaxy may be tidally disturbed. The uncertainty in the slope is determined with rescaled errors such that the reduced $\chi^2 = 1.0$. The shallow slope is consistent within our errors with the slope determined from the data of Faber et al. (1989), which give $L_B \propto \sigma^{2.61\pm0.08}$ using their R-distances. For comparison, the K-band slope is significantly steeper (Pahre, Djorgovski, & de Carvalho 1998).

3.2. *Tully-Fisher Relation*

The relation between the circular velocity and total luminosity, known as Tully-Fisher (1977, hereafter TF) relation, is observationally well established for spiral galaxies. From the K+2000 dynamical analysis, we now know circular velocities also for elliptical galaxies and can thus investigate whether ellipticals also follow a TF relation. We use the $v_c^{\max}$ variable and errors from § 2 and integrated total B_T^i as before, for the 21 galaxies analyzed in K+2000. These data points are shown in the middle and lower panels of Figure 7. From a least-squares fit in both variables we obtain a B-band TF-slope of -5.92 ± 1.21, corresponding to

$$L_B \propto (v_c^{\max})^{2.37\pm0.48}, \tag{3}$$

again excluding NGC 4486B and using rescaled errors to estimate the uncertainty. The derived slope is consistent with the Faber-Jackson relation and the $v_c^{\max}$–$\sigma_{0.1}$ relation discussed in § 2.3. The zero point of the relation is given by

$$v_c^{\max} = 493 L_{11}^{0.42} \text{ km s}^{-1}, \tag{4}$$

where $L_{11} = L_B/10^{11} h_{0.65}^{-2} L_{\odot,B}$ and $h_{0.65} = H_0/65$ km s^{-1} Mpc^{-1}; this implies $v_c^{\max,*} \simeq 303$ km s^{-1} for an L^*-elliptical galaxy, using a corrected $M_B^*(B_T^0) = -20.8$ [$L_B^*(B_T^0) = 10^{10.5} L_{B,\odot}$] for $H_0 = 65$ km s^{-1} Mpc^{-1} from Fukugita & Turner (1991). The corresponding $\sigma_{0.1}^* \simeq 195$ km s^{-1}.

We have also included the S0s from Neistein et al. (1999) in the TF plot. We took the circular velocities corrected for asymmetric drift from their Table 1, column (13), but used the B-band luminosities from the RC3 (de Vaucouleurs et al. 1991) rescaled to our distance scale (using distances from Faber et al. 1989 where available: NGC 584, 1052, 2768, 3115, 4649, and for the remaining S0 galaxies redshifts with respect to the CMB frame and $H_0 = 65$ km s^{-1} Mpc^{-1}). The S0's join smoothly with the ellipticals in the TF plot. The fitted slope for both samples together is slightly steeper (-7.09 ± 0.91) than for the ellipticals alone, but the two slopes are consistent within their errors.

The lower panel of Figure 7 shows the comparison of the elliptical and spiral galaxy TF relations. The data points and the heavy least-squares fit line repeat the B-band elliptical galaxy relation. The two lower dashed lines show the Cepheid-calibrated B-band Tully-Fisher relations for spiral galaxies from Federspiel, Tammann, & Sandage (1998) and Sakai et al. (2000), which are in mutual agreement to a few tenths of a magnitude over the range of interest here. The TF relations of these authors are given in terms of H I line width measured at 20% peak flux and were converted to $v_c^{\max}$ by using Figure 18 of Rubin, Waterman, & Kenney (1999), which shows that the inclination-corrected $W_{20} = 2.0 v_c^{\max}$ to within the errors. The dotted line shows the r-band relation from Courteau & Rix (1999), converted to the B-band using the color magnitude relation they give for their sample of spirals and converted to our $H_0 = 65$ km s^{-1} Mpc^{-1} distance scale. Their velocities $v_{2.2}$ were used directly as $v_c^{\max}$. The average of the spiral galaxy slopes is somewhat steeper than the elliptical galaxy relation, but given the large scatter in the latter and between the spiral galaxy slopes, this difference is marginal.

Federspiel et al. (1998) applied their calibration to a complete sample of Virgo cluster spiral galaxies to derive a mean cluster distance modulus of $(m-M)_0 = 31.58 \pm 0.24$ mag. According to Faber et al. (1989), the Virgo cluster center is at a distance of $v = 1333$ km s^{-1}. By using relative distances from Faber et al. (1989) (the R-values of their Tables 3 and 4) and a Hubble constant of $H_0 = 65$ km s^{-1} Mpc^{-1} to obtain the absolute magnitudes B_T^i for our elliptical galaxies, we have thus implicitly assumed a Virgo cluster distance modulus of $(m-M)_0 = 5 \log (1333/65) + 25 = 31.56$ mag, which is identical to the spiral galaxy mean Virgo distance modulus of Federspiel et al. (1998). Thus, the zero points of the Cepheid-calibrated TF relations are directly comparable to our elliptical galaxy TF. In fact, this comparison need not make any assumption about absolute distances; the only assumption made is that the centroid of the Virgo cluster spiral galaxy sample coincides with the Virgo cluster ellipticals as given by Faber et al. (1989); the relative distances between the ellipticals in our sample are then also fixed. Therefore, the offset between elliptical and spiral galaxies in Figure 7 can be regarded as one in *apparent magnitude*. Its value depends only on having used the correct relative distance of the two systems.

Taking an average over the different spiral galaxy TF relations in the plot, we conclude that, at a given circular velocity, elliptical galaxies are about 1 mag fainter in B than spiral galaxies. Put differently, at given luminosity elliptical galaxies have higher circular velocities than spirals by about 0.2 dex. This difference decreases slightly if instead of maximum circular velocities we use the halo velocities of our models. To see whether this difference is smaller in the redder R band, where elliptical galaxies should be relatively brighter, we have plotted in the lower panel of Figure 7 the R-band TF relation expected from the B-band fit and the color-magnitude relation from the EFAR sample (Saglia et

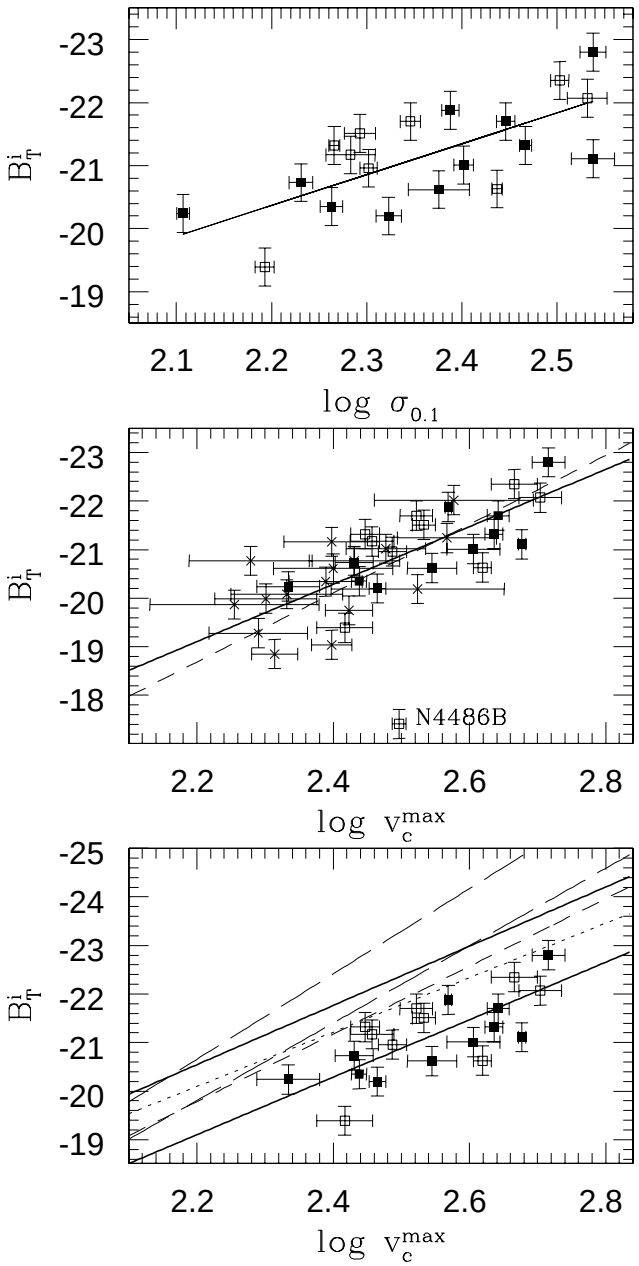

FIG. 7.—*Top*: Faber-Jackson relation for our sample of elliptical galaxies. Filled squares and open squares show galaxies from the EK and BSG subsamples of K+2000. $\sigma_{0.1}$ is the averaged velocity dispersion inside $0.1R_e$ (see text); this is not available for NGC 4486B. The solid line shows a least-squares fit. *Middle*: Tully-Fisher relation for the elliptical galaxies from K+2000 (same point styles) and S0s from Neistein et al. (1999) (*stars*). Ellipticals and S0s form a smooth sequence; the slope of the elliptical galaxies alone (*solid line*, fit excludes NGC 4486B) is marginally shallower than the slope for the combined sample (*dashed line*). *Bottom*: Comparison of elliptical and spiral galaxy Tully-Fisher relations. Ellipticals: Data points and least-squares fit line repeat the *B*-band relation. The upper heavy line shows this relation shifted to the *R* band, using the color-magnitude relation given in the text. Spirals: Cepheid-calibrated *B*-band Tully-Fisher relations from Federspiel et al. (1998, *short-dashed line*) and Sakai et al. (2000, *lower long-dashed line*), Cepheid-calibrated *R*-band relation from Sakai et al. (2000, *upper long-dashed line*), and *r*-band relation from Courteau & Rix (1999, *dotted line*) shifted to the *B* band using the color-magnitude relation for their spirals.

al. 1997a), $B-R = -0.030(R + 22.5) + 1.50$ (*upper solid line*), to be compared to the *R*-band Cepheid-calibrated relation from Sakai et al. (2000), plotted as upper long-dashed line. With respect to the Sakai et al. relations in *R* and *B*, the offset is indeed ~ 0.4 mag smaller in *R* than in *B* at log $v_c^{max,*}$, but note the different slopes.

In Figure 8 we show the residuals from the elliptical galaxy TF relation versus the mean velocity anisotropy β_{mean} and the effective radius. There is no obvious correlation with β_{mean}. On the other hand, the plot against R_e does show a correlation, which reflects the existence of the fundamental plane (see next section).

In summary, elliptical galaxies follow a Tully-Fisher relation, with a *B*-band slope that is marginally shallower than the slope for spiral galaxies, and zero point such that an L^*-elliptical has a circular velocity $v_c^{max,*} \simeq 300$ km s^{-1}. At given circular velocity, elliptical galaxies are about 1 mag fainter in *B* than spiral galaxies.

3.3. *Baryonic Tully-Fisher Relation*

Since the stellar mass-to-light ratios of elliptical galaxies vary significantly with luminosity (see § 3.5), it may be more revealing to plot luminous mass against circular velocity than luminosity. The mass of the X-ray emitting gas in ellipticals is only a few percent even for luminous galaxies (Forman, Jones, & Tucker 1985; Sarazin 1997). The stellar mass is thus nearly equal to the total baryonic mass. Figure 9 shows stellar mass $M_* = M/L_{central} \times L_B$ versus maximum circular velocity for our sample of elliptical galaxies, where $M/L_{central}$ is the maximum M/L allowed by the kinematic data. The steeper dotted line in the diagram is the best-fit spiral galaxy baryonic Tully-Fisher relation from McGaugh et al. (2000), including stellar and gaseous mass. Their stellar masses were determined from red and NIR luminosities, using M/L-values based on population models

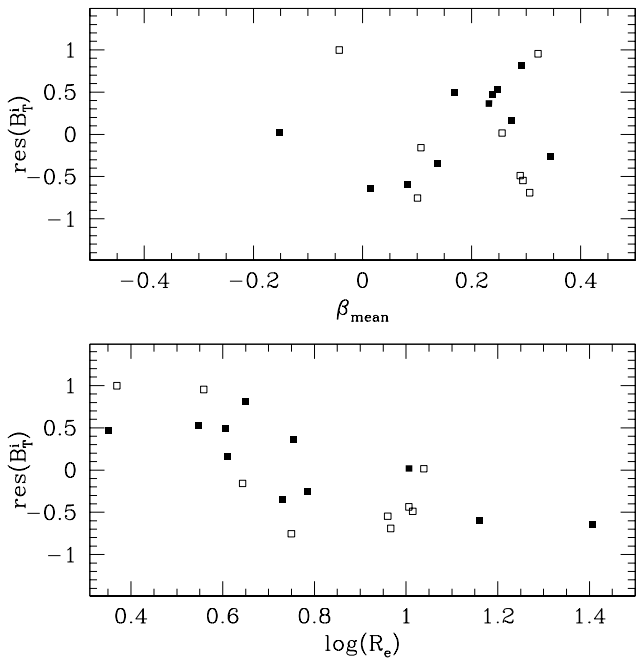

FIG. 8.—*Top*: The residuals in B_T from the Tully-Fisher relation for the elliptical galaxies vs. their mean anisotropy β_{mean}, excluding NGC 4486B. *Bottom*: The residuals in B_T from the elliptical galaxy Tully-Fisher relation vs. effective radius *Re*.

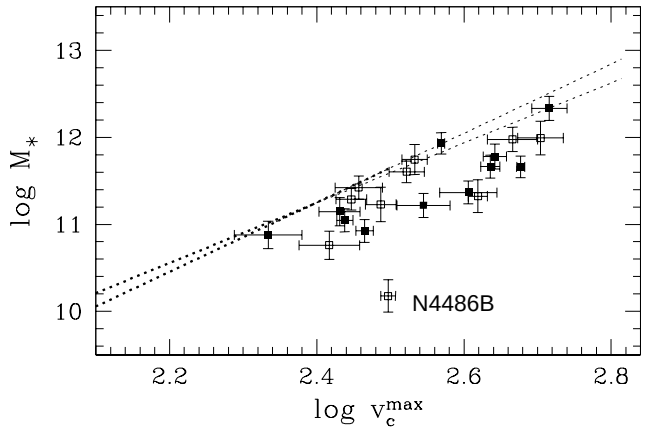

FIG. 9.—Luminous mass in stars vs. maximum circular velocity for our sample of elliptical galaxies. The dotted lines show the baryonic mass–rotation velocity relations for spiral galaxies from McGaugh et al. (2000, *steeper*) and Bell & de Jong (2001, *shallower*). The heavy parts of these lines cover the range of the fitted spiral galaxy data.

(constant star formation rate, Salpeter IMF, such that $M/L_K = 0.8\ M_\odot/L_{\odot,K}$, $M/L_B = 1.4\ M_\odot/L_{\odot,B}$). According to McGaugh et al. (2000) these model M/L are consistent with maximum disk fits for the bright galaxies. The shallower dotted line is the spiral galaxy line from Bell & de Jong (2001). This is based on luminosities in several passbands and M/L ratios determined from evolution models, which use an IMF containing fewer low-mass stars than a Salpeter IMF, as suggested by recent observations in the Galaxy (e.g., Gould, Bahcall, & Flynn 1997; Holtzman et al. 1998) and so that maximum disk M/L-values are not exceeded. Both spiral galaxy relations apparently predict very similar baryonic masses for the circular velocities of interest here. The thin parts of both lines are extrapolated from the thick parts with spiral galaxy data.

In Figure 9 elliptical galaxies fall below the spiral galaxy lines by a factor of about 2 in the mean. Note that the offset to the spiral galaxies cannot be explained by luminosity errors for our ellipticals alone (Saglia et al. 1997b). The diagram is changed little if instead of $v_c^{\max}$ we use the on average slightly lower circular velocities at $1R_e$ for the elliptical galaxy points. Note, however, that there is only a partial overlap in velocity for the spiral and elliptical galaxy samples. With the present data the case for elliptical galaxies having indeed lower baryonic mass than spiral galaxies of the same circular velocity is therefore not entirely clear.

It is noteworthy, however, that the baryonic masses of elliptical galaxies from dynamics are if anything slightly lower than the baryonic masses of spiral galaxies from realistic stellar population models, in the region where both distributions overlap. This suggests that the underlying assumption, that ellipticals are described by maximum stellar mass models is approximately correct and, hence, that elliptical galaxy halos have indeed fairly flat cores: in hierarchical models in which ellipticals form through merging, a continuity between spirals and ellipticals would be expected. Near-maximal M/L in ellipticals are in line with results for the Milky Way (Gerhard 1999) and barred galaxies (Debattista & Sellwood 1998; Weiner, Sellwood, & Williams 2001), where independent dynamical constraints on the luminous mass favor near-maximal disks, while the situation is less clear for luminous unbarred spirals (see, e.g., Athanassoula, Bosma, & Papaioannou 1987; Courteau & Rix 1999; Salucci & Persic 1999; Bell & de Jong 2001).

3.4. *Fundamental Plane*

In the three-dimensional space defined by central velocity dispersion, effective surface brightness (I_e), and effective radius (R_e) elliptical galaxies fall on a "fundamental plane" (FP; Dressler et al. 1987; Djorgovski & Davis 1987). The existence of the FP is thought to be a consequence of the virial theorem together with a systematic relation of M/L on luminosity (Dressler et al. 1987; Faber et al. 1987). Figure 10 shows the FP projection after Jørgensen, Franx, & Kjærgard (1996) for our sample of ellipticals. Effective radii R_e are taken from Table 3 of K+2000, effective surface brightnesses I_e are computed from the (corrected) SB-profiles integrated to $1R_e$ (Table 4 of K+2000), and for the central velocity dispersion we have used the $\sigma_{0.1}$ defined in § 2.3. The best-fitting line of slope 1.0 is shown along with the data in the top panel of Figure 10. The residuals with respect to the best-fitting line are plotted in the bottom panel against the velocity anisotropy $\beta_{\rm mean}$. As Figure 10 shows, these galaxies follow the FP well and the residuals are not correlated with $\beta_{\rm mean}$. The rms scatter in log R_e is 0.084, excluding NGC 4486B. If we fit the slope as well, it is 0.924 ± 0.069 and the scatter becomes 0.082.

In the previous section, we have remarked on the correlation of the residuals from the elliptical galaxy TF relation with R_e. This implies that also in the $v_c^{\max} - R_e - B_T^i$ space elliptical galaxies fall on a fundamental plane. Because $v_c^{\max}$ is very tightly correlated with $\sigma_{0.1}$ (Fig. 6), the resulting plane is very similar to the standard FP.

3.5. *Luminous Mass-Luminosity Relation*

From the variables (R_e, $\sigma_{0.1}$, I_e) one may define a luminosity $L = c_L I_e R_e^2$ and mass $M_{FP} = 3c_M R_e \sigma_{0.1}^2/G$. As first

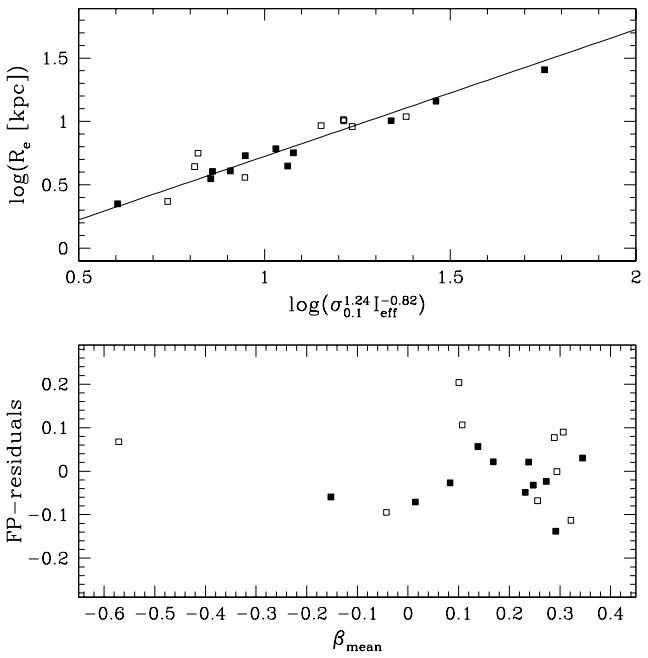

FIG. 10.—*Top*: *B*-band fundamental plane for the sample of elliptical galaxies from K+2000. The parameterization of the FP is taken from Jørgensen et al. (1996). The line shows the best fit with fixed slope 1.0. *Bottom*: Residuals of the fit plotted against mean anisotropy β. Symbols as in Fig. 5.

pointed out by Faber et al. (1987), the virial theorem would then predict $I_e \propto \sigma_{0.1}^2 R_e^{-1}$, provided the mass-to-light ratio and the structure constants c_L and c_M are identical for all galaxies. The tilt of the FP with respect to the virial relation therefore implies either a luminosity dependence of M/L or some deviation of the family of elliptical galaxies from homology. In the former case and if the FP is $R_e \propto \sigma_{0.1}^{\alpha} I_e^{\beta}$, we would expect $M/L \propto L^{(2-\alpha)/2\alpha} I_e^{(-2-\alpha-4\beta)/2\alpha}$. For the present sample $\alpha = 1.15$ and $\beta = -0.758$, so that one obtains $M/L \propto L^{0.37} I_e^{-0.05}$.

From our dynamical models we have derived central and cumulative B-band mass-to-light ratios from observed SB-profiles and kinematics. The central M/L_B corresponds to the mass-to-light ratio of the stellar population, on the assumption of a maximum stellar mass (minimum halo) model in which the luminous stars provide as much mass in the central parts as is allowed by the kinematic data. These M/L_B-values have no residual correlation with anisotropy (Fig. 11); this is expected as the anisotropy was taken into account in the modeling.

Figure 12 shows the ratio of the dynamically determined cumulative mass at $1R_e$, including any dark mass that may be necessary up to this radius, and the FP mass, $M_{FP} \equiv 3R_e\sigma_0^2/G$, for galaxies with data to beyond R_e. This ratio measures the structure constant c_M. From the figure it is clear that there is no systematic trend of c_M with circular velocity or mass. Because both photometry and dynamical anisotropy were taken into account in the modeling, this shows that the dynamical nonhomology mechanism proposed by Graham & Colless (1997) is not the main cause for the tilt of the FP. On the contrary, the dynamical structure of elliptical galaxies is remarkably uniform (Fig. 6), and no correlation was found between M/L and anisotropy (Fig. 11).

Figure 13 shows the dynamically determined mass-to-light ratios against luminosity. The upper panel of Figure 13 shows the central M/L_B, i.e. the inferred mass-to-light ratio of the stellar population in our models. The range in central M/L_B is about a factor of 3. The lower panel shows the cumulative mass-to-light ratio at R_e. The scatter in these diagrams is comparable to each other, and galaxies with particularly low or high M/L_B correspond almost one by one. For the EK sample the scatter is similar to the scatter in the FP mass-luminosity relation while for the BSG sample it is somewhat larger, as might be expected.

Contrary to the range in central M/L_B, which is fixed by the dynamical models, the actual slope of the $M/L - L$ relation also depends on the extrapolation used to derive the total luminosity; the K+2000 values were derived from the photometry using a de Vaucouleurs law. The fitted slopes are slightly steeper than the predicted FP relation. For the EK sample they are for $M/L_{\rm central}$: 0.57 ± 0.11 when the errors are rescaled to $\chi^2 = 1.0$, and for $M/L(R_e)$: 0.59 ± 0.09 with $\chi^2 = 0.7$. For the total sample (excluding NGC 4486B) they are for $M/L_{\rm central}$: 0.65 ± 0.09 when $\chi^2 = 1.0$, and for $M/L(R_e)$: 0.67 ± 0.15 when $\chi^2 = 1.0$. These slopes are different from the predicted FP slope by 1.5–2.5 times the σ of the M/L fit, and they are either influenced by small number effects (for the EK sample) or by outlying data points (for the full sample). They thus appear

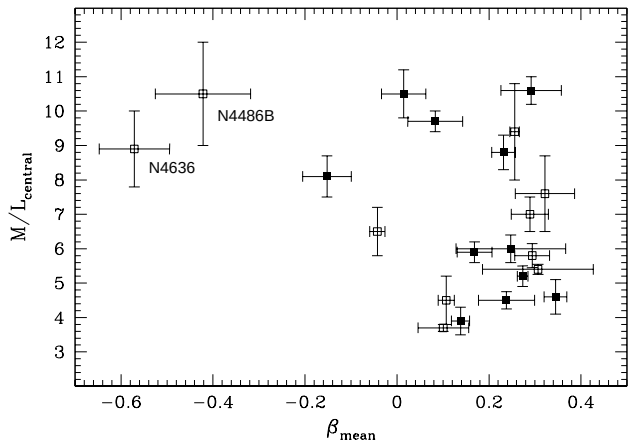

FIG. 11.—Central B-band M/L vs. mean velocity anisotropy β. No correlation is found.

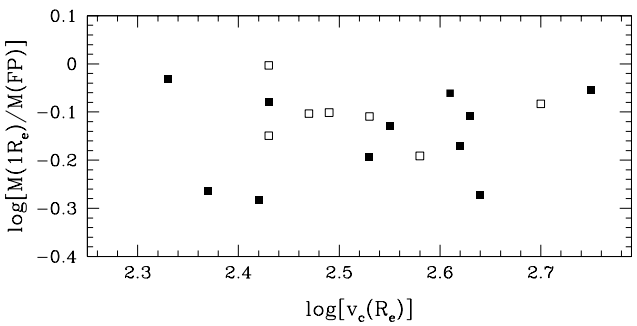

FIG. 12.—Ratio of the cumulative mass $M(R_e)$, luminous and dark, to FP mass $3R_e\sigma_0^2/G$, vs. circular velocity at R_e. Symbols as in Fig. 5.

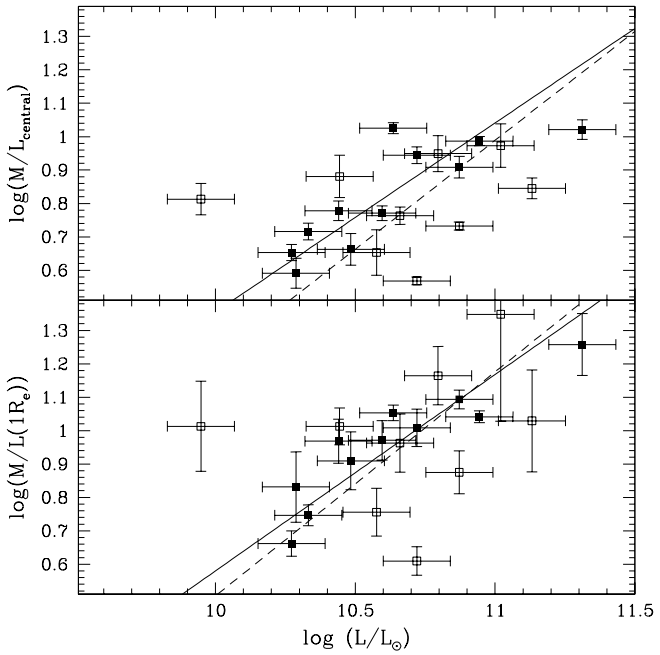

FIG. 13.—Mass-to-light ratios as a function of luminosity. The top panel shows the log of the central B-band M/L vs. total L_B. The bottom panel shows the cumulative $M/L_B(R_e)$ at one effective radius vs. L_B, including any dark mass. Symbols are as in Fig. 5. Total L_B and errors as in Fig. 7. The errors on the mass-to-light ratios correspond to one-half the range in the M/L profiles of K+2000, as determined by dynamical models bounding the respective confidence interval for each galaxy. In each panel two least-squares fits are shown, for all galaxies in the sample but NGC 4486B (*dashed lines*), and for the EK subsample only (*solid lines*). The slopes of these two fits are not significantly different.

still consistent with the predicted FP slope. Figures 6 and 12, which demonstrate the dynamical similarity of our galaxies, also suggest that the difference may not in fact be significant.

From these results we conclude that the M/L variations with luminosity indicated by the tilt in the fundamental plane are real. The inferred FP M/L ratios for our sample of ellipticals correspond to the dynamically measured M/L-values for the stellar populations, assuming a minimal halo, and they are not due to a nonhomologous dynamical structure changing gradually with luminosity. It is still possible, however, that photometric nonhomology influences the slope of the $M/L-L$-relation. The trend of M/L with L is also not caused by an increasing fraction of dark matter as luminosity increases, unless two-thirds of the luminous mass in the cores of the most massive galaxies is dark matter, and luminous elliptical galaxies are then significantly short of baryons compared to spirals (see § 3.3 and Fig. 9). The change of M/L with L is therefore most likely due to the population itself.

4. CENTRAL M/L AND STELLAR POPULATIONS

The question of what causes the variation with luminosity of the M/L-values observed in ellipticals has been discussed at length in the literature, without any fully satisfactory answer. Systematic deviations from homology have been argued to play a role (Pahre et al. 1998), but as discussed above this is not a viable solution. It is possible to fit the trend observed in the B band as a metallicity sequence of an old stellar population (Maraston 1999). However, the M/L-values in the K band which this model would predict are independent of metallicity, and therefore no correlation with K-band luminosity should be expected, contrary to what is observed (Pahre et al. 1998). Forbes, Ponman, & Brown (1998) and Forbes & Ponman (1999) analyze the ages determined for 88 galaxies and conclude that the observed correlation between age and luminosity is far too weak to explain the observed M/L trend with luminosity in any band.

Here we explore whether stellar population models can reproduce the central B-band M/L_B-values derived from our (minimum halo) dynamical models. We compare these M/L_B-values with the predictions of stellar populations models in Figure 14. We use the stellar population models of Maraston (1998), as employed in Saglia et al. (2000b), to interpolate the M/L_B expected for a simple stellar population of given metallicity and age. These models take into account stellar evolution mass loss, i.e., they include in the mass budget the masses of stellar remnants, but not the mass losses of the progenitor stars. This is different from what is done by, e.g., Worthey (1994) or Bruzual & Charlot, in preparation, where the total initial mass is conserved. In addition to the classical Salpeter IMF (with power-law exponent $\gamma = -2.35$ independent of stellar mass), we consider two additional choices for the IMF: the recent comprehensive determination of Kroupa (2000), indicating that the low-mass stars could be less numerous (his eq. [2]: $\gamma = -1.3$ for $m < 0.5\ M_\odot$, $\gamma = -2.3$ at larger masses), and the more extreme IMF of Gould, Bahcall, & Flynn (1997, hereafter GBF), where a flatter slope at lower masses is suggested (after correction for binaries, $\gamma = -0.9$ for $m < 0.6\ M_\odot$, $\gamma = -2.21$ for $0.6 < m < 1$ and $\gamma = -2.35$ for $m > 1\ M_\odot$). For all three IMFs we use a lower stellar mass cutoff of $0.1\ M_\odot$.

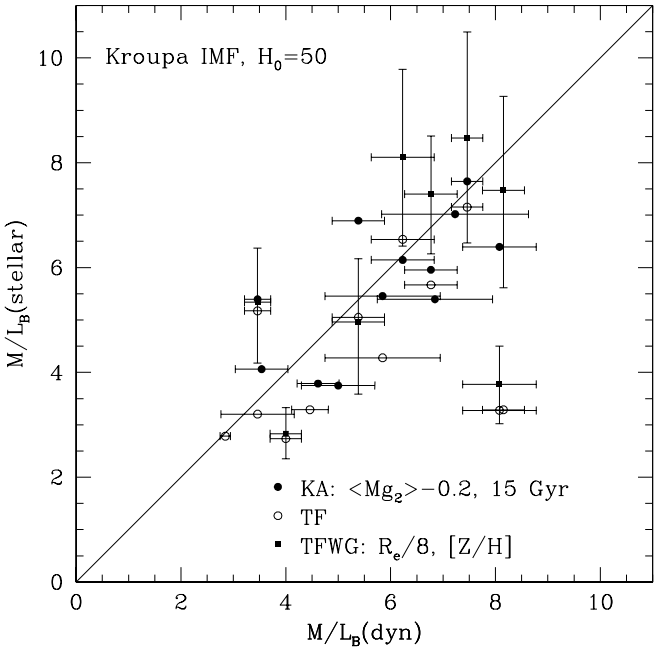

FIG. 14.—Comparison between the dynamical estimates of the central B-band M/L (transformed to $H_0 = 50$ km s^{-1} Mpc^{-1}) with the predictions of stellar population models of Maraston (1998), using Kroupa's (2000) IMF. Metallicities and ages used in the models are taken from Kobayashi & Arimoto (1999, *filled circles*), Terlevich & Forbes (2000, *open circles*), Trager et al. (2000a, 2000b, *filled squares*).

As input we use ages and metallicities as derived by Kobayashi & Arimoto (1999), Terlevich & Forbes (2000) and Trager et al. (2000a). Such data are available from at least one study for 17 out of 21 of our galaxies.

Kobayashi & Arimoto (1999) derived mean metallicities inside $1R_e$, considering line index gradients. We use values as given in their Table 2. These are derived from the Mg_2 line, assuming an age of 17 Gyr. The M/L_B-values shown in Figure 14 are determined by reducing their metallicities by 0.2 dex (to correct for the Mg/Fe overabundance) and for an age of 15 Gyr.

Terlevich & Forbes (2000) compiled a catalog of high-quality absorption line measurements for galaxies and derived separate age and metallicity estimates using Worthey (1994) models.

Trager et al. (2000a) determined ages and metallicities after applying a correction for the Mg/Fe overabundance to the line indices. We use their ages and metallicities for the inner $R_e/8$ data points, and average over the four models considered by these authors, for all galaxies except NGC 1399. For this galaxy we use the new age and metallicity determination by Trager et al. (2000b); for the other galaxies the new determinations agree with the previous values within the errors.

Table 1 lists the resulting stellar population M/L_B-values with each of the three IMFs. Figure 14 shows the comparison of the stellar M/L_B-values determined with Kroupa's (2000) IMF with the dynamical M/L_B-values, rescaled to $H_0 = 50$ km s^{-1} Mpc^{-1}, which gives the best overall agreement. The galaxy-by-galaxy comparison after this rescaling is reasonable within the errors. Only two objects are particularly deviant: NGC 315, where the dynamical value is a factor 2 larger than the stellar population estimates based on Terlevich & Forbes (2000) and Trager et al. (2000a) but

TABLE 1

THE M/L_B-VALUES OF THE STELLAR POPULATIONS IN SOLAR UNITS, USING THE MODELS OF MARASTON (1998)

		SALPETER			KROUPA			GBF		
GALAXY (1)	DYN. (2)	KA (15 Gyr) (3)	TF (4)	TFWG (R_e/8) (5)	KA (15 Gyr) (6)	TF (7)	TFWG (R_e/8) (8)	KA (15 Gyr) (9)	TF (10)	TFWG (R_e/8) (11)
NGC 315.....	10.5	10.1	5.8	6.5	6.4	3.3	3.8	5.0	3.2	3.5
NGC 1399.....	10.6	...	5.8	12.6	...	3.3	7.5	...	3.2	6.8
NGC 2434.....	6.0	5.8	...	...	3.8	...	...	3.0	...	...
NGC 3193.....	4.5	...	5.1	...	...	3.2	...	...	2.5	...
NGC 3379.....	4.5	8.4	8.6	8.8	5.4	5.1	5.3	4.2	4.5	4.6
NGC 3640.....	3.7	...	4.4	...	...	2.8	...	...	2.2	...
NGC 4168.....	5.8	...	5.2	...	...	3.3	...	...	2.6	...
NGC 4278.....	7.6	8.5	6.9	...	5.5	4.3	...	4.3	3.5	...
NGC 4374.....	8.8	9.3	9.1	11.8	6.0	5.7	7.4	4.7	4.6	6.0
NGC 4472.....	7.0	10.9	8.5	8.3	6.9	5.1	5.0	5.4	4.5	4.4
NGC 4486.....	9.4	11.1	...	...	7.0	...	...	5.5	...	...
NGC 4494.....	6.5	5.8	...	...	3.8	...	...	3.0	...	...
NGC 4636.....	8.9	8.4	...	...	5.4	...	...	4.2	...	...
NGC 5846.....	9.7	12.1	11.9	13.5	7.7	7.2	8.5	6.0	6.2	6.8
NGC 6703.....	5.2	...	4.8	4.9	...	2.7	2.8	...	2.7	2.7
NGC 7192.....	4.6	6.3	...	...	4.1	...	...	3.2	...	...
NGC 7626.....	8.1	9.6	10.6	13.0	6.2	6.6	8.1	4.8	5.4	6.6

NOTES.—Col. (1) gives the galaxy name, col. (2) the M/L_B of the luminous component from our dynamical analysis, using $H_0 = 65$ km s^{-1} Mpc^{-1}, col. (3) the M/L_B derived using the metallicities of KA (Kobayashi & Arimoto 1999) with 15 Gyr age, col. (4) using ages and metallicities from TF (Terlevich & Forbes 2000), and col. (5) using ages and metallicities inside (R_e/8) of TFWG (Trager et al. 2000a, 2000b). Cols. (3), (4), and (5) are computed for a Salpeter IMF. Cols. (6), (7), and (8) repeat cols. (3), (4), and (5), but for the Kroupa (2000) IMF. Cols. (9), (10), and (11) are the same for the GBF IMF.

is in agreement with the value obtained from Kobayashi & Arimoto (1999), and NGC 1399, where M/L_B(dyn) is again a factor 2 larger than the stellar M/L_B based on Terlevich & Forbes (2000) but agrees with the value derived from Trager et al. (2000b). This discrepancy is due to the rather low ages (5 Gyr) assigned there, which is also in conflict with the determinations of Maraston & Thomas (2000).

Similar plots are obtained for the Salpeter and the GBF IMFs, when distances are scaled to an optimal $H_0 = 75$ km s^{-1} Mpc^{-1} for the former and $H_0 = 40$ km s^{-1} Mpc^{-1} for the latter case. These diagrams show that the dynamical M/L_B obtained with $H_0 = 65$ km s^{-1} Mpc^{-1} are $\approx$30% larger than the stellar M/L_B-values with the Kroupa (2000) IMF, $\approx$60% larger with the GBF IMF, and $\approx$20% smaller than the stellar M/L_B-values with the Salpeter IMF. Note that an IMF flatter than Salpeter for $m > 1\ M_\odot$ produces stellar M/L-values larger than the Salpeter values.

We conclude that our dynamical M/L_B-values, based on models maximizing the contribution of the luminous component, are compatible with those predicted by stellar population models, within the uncertainties in the distance scale and the poorly known fraction of low-mass stars present in giant ellipticals. Only in the case that (i) an IMF as flat at low stellar masses as that of GBF is applicable to our elliptical galaxies, and simultaneously (ii) a short distance scale ($H_0 \simeq 80$ km s^{-1} Mpc^{-1}) turns out to be correct, would we have overestimated the luminous masses by as much as a factor $\approx$2 by making the assumption of maximum stellar, or minimum dark halo mass. For lower values of H_0 and/or the other IMFs investigated the difference is smaller. For comparison, recall that to explain the tilt of the FP as due to an increasing fraction of dark matter with luminosity, we would require the stellar mass in the most luminous ellipticals to be only one-third of the inferred dynamical mass. Furthermore, the ratio of M/L_B(dyn)/M/L_B(stellar) for this sample of elliptical galaxies does not correlate with luminosity.

Together with the results of § 3 this suggests that the tilt of the FP is a stellar population effect. Most likely the main driver is metallicity, but then a secondary population effect is needed to explain the K-band tilt (Pahre et al. 1998). A larger sample of galaxies with detailed dynamical modeling also of the K-band profiles will be needed to decide whether this is the final answer to the problem of the tilt of the fundamental plane.

5. MASS-TO-LIGHT RATIOS AND MINIMUM HALO PROPERTIES

In this section we first show that the dynamical models imply significant radial M/L variations in elliptical galaxies. Because the implied *local* mass-to-light ratios are large, we argue that these are the signature of dark matter halos. Based on the result of the previous section, that the dynamically determined central M/L_B-values for our ellipticals are consistent with the stellar population M/L_B-values, we use the dynamical models to delineate the decomposition of the elliptical galaxy circular velocity curves (CVCs) into luminous and dark contributions, and finally study the properties of the implied minimum halos.

5.1. *Global and Local Mass-to-Light Ratios*

Figure 15 shows the radial profiles of cumulative $M(r)/L_B(r)$ for all galaxies in the two subsamples, as derived from the respective "best model" CVC (Fig. 1) and luminosity profile. There is considerable variety in these cumulative M/L_B-profiles; even within the galaxies with extended kinematics, the ratio of cumulative M/L_B at the outer data boundary to the central value ranges from consistent with 1 to $\lesssim$2 (see also Table 7 of K+2000). This suggests a corresponding spread in the efficiency of dissipational segrega-

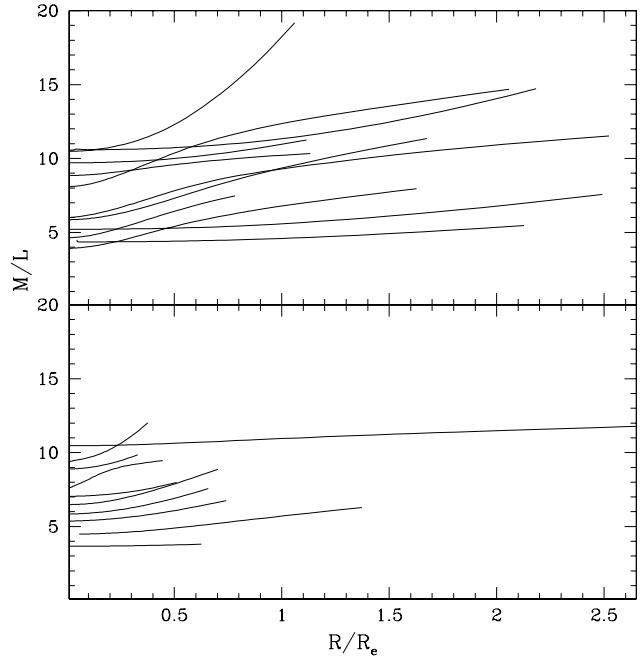

FIG. 15.—Cumulative B-band $M(r)/L_B(r)$ as function of radius. *Top*: EK galaxies; *bottom*: BSG galaxies.

tion and angular momentum loss of the stellar and gaseous component in the dark matter halo during the formation process.

Even though the gradients in cumulative M/L_B are modest, those in the *local* mass-to-light ratio $\rho(r)/j_B(r)$ are not. [Here $\rho(r)$ and $j_B(r)$ are the inferred mass and luminosity densities]. Because these local ρ/j-ratios are less certain than the cumulative M/L_B-values we show these in Figure 16 only for the best cases from the EK-subsample with extended kinematics. As the figure shows, these local M/L_B-values become large $\sim$20–30 in the modeled outer parts of these galaxies. This, and corroborating evidence from X-ray data (e.g., Matsushita et al. 1998; Loewenstein & White 1999) argues strongly that the measured M/L variations are not due to a slow outward change of the stellar population, but instead imply dark matter halos similar to those inferred in spiral galaxies, where the component contributing most of the mass, baryonic or not, is very different from a normal stellar population.

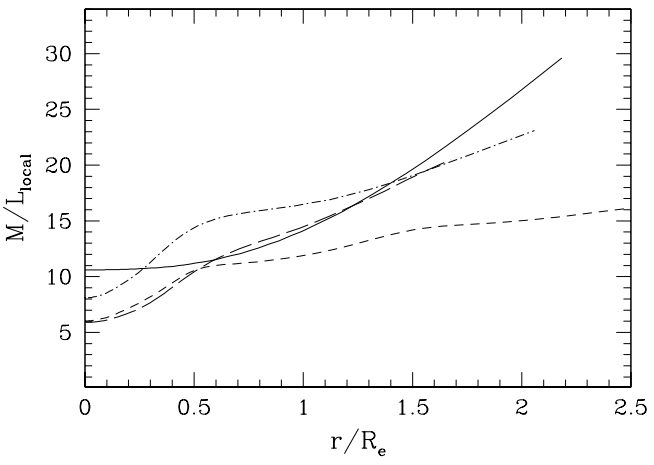

FIG. 16.—*Local* B-band M/L_B as function of radius for the four most reliable galaxies from the EK sample: NGC 1399 (*solid line*), NGC 7626 (*dot-dashed line*), NGC 7507 (*long-dashed line*), and NGC 2434 (*short-dashed line*), over the range of the modeled kinematic data.

5.2. *Circular Velocity Curve Decomposition*

Thus, as for spiral galaxies, it is of interest to analyze the relative contributions of the luminous and dark matter components to the CVCs in Figure 1. In doing this we assume that the M/L_B of the luminous component is constant with radius and has the maximal value allowed by the kinematic data, providing nearly all the mass in the center. The dynamical models used by K+2000 to analyze the kinematic data were built on this assumption, but once the CVCs are determined, the luminous component could in principle be assigned less mass a posteriori. The discussion in § 4 has shown that the maximum central M/L_B-values determined for our ellipticals by K+2000 are consistent with the M/L_B-values expected for the stellar population of these galaxies, within the uncertainties in the distance scale and the lower mass IMF. Figure 9 has also shown that even with maximal M/L_B elliptical galaxies have if anything slightly lower baryonic mass than spiral galaxies of the same circular velocity.

Figure 17 shows the total circular velocity curves from Figure 1 for all galaxies in the high-quality EK-sample, and the respective contributions from the maximum luminous and corresponding minimum dark halo components. At $1R_e$, the halo contributes between 1/4 to 2/3 of the circular velocity in these "best" dynamical models, corresponding to between 10%–40% of the integrated mass. All curves are plotted to radii of $5R_e$, extrapolating the models beyond the radial range of the data. The case of NGC 315 (where the outer rise of the CVC is due to modeling problems, see K+2000) shows that such extrapolation can lead to large errors. However, in cases where X-ray data or planetary or globular cluster velocities were available, the "best" models of K+2000 matched the independent mass estimates from these outer data very well. Figure 17 shows that within the framework of the models, luminous and dark matter reach equal interior mass at $\sim$2–4R_e, and at $5R_e$ the halo is predicted to dominate in all models except in one case. As in spiral galaxies, the combined rotation curve is flatter than that for the individual components ("conspiracy"); this is already seen within the radial range of the kinematic data.

The last panel of Figure 17 repeats the CVC decomposition for NGC 2434 with a luminous $M/L_B = 3.4$ instead of the maximum $M/L_B = 6.0$. This is the average of the population values obtained for this galaxy with the Kroupa and GBF IMFs (see Table 1). The lower M/L_B leads to a significantly denser halo; the decomposition in this case is comparable to those of Rix et al. (1997) with a Navarro, Frenk & White (1996, hereafter NFW) halo mass distribution. This example suggests (i) that the kinematic data for the K+2000 sample could presumably have been fitted also by using these halo models and (ii) that the resulting lower M/L_B-values for the luminous components would be near the lower end of the range consistent with the stellar population models of § 4. However, in this case, ellipticals would move further down in Figure 9: in the models of Rix et al. (1997) with a NFW halo for NGC 2434 the M/L for the luminous component is another (for the same distance) factor of 1.5 smaller than the maximum M/L found by K+2000, which had already placed NGC 2434 by a factor

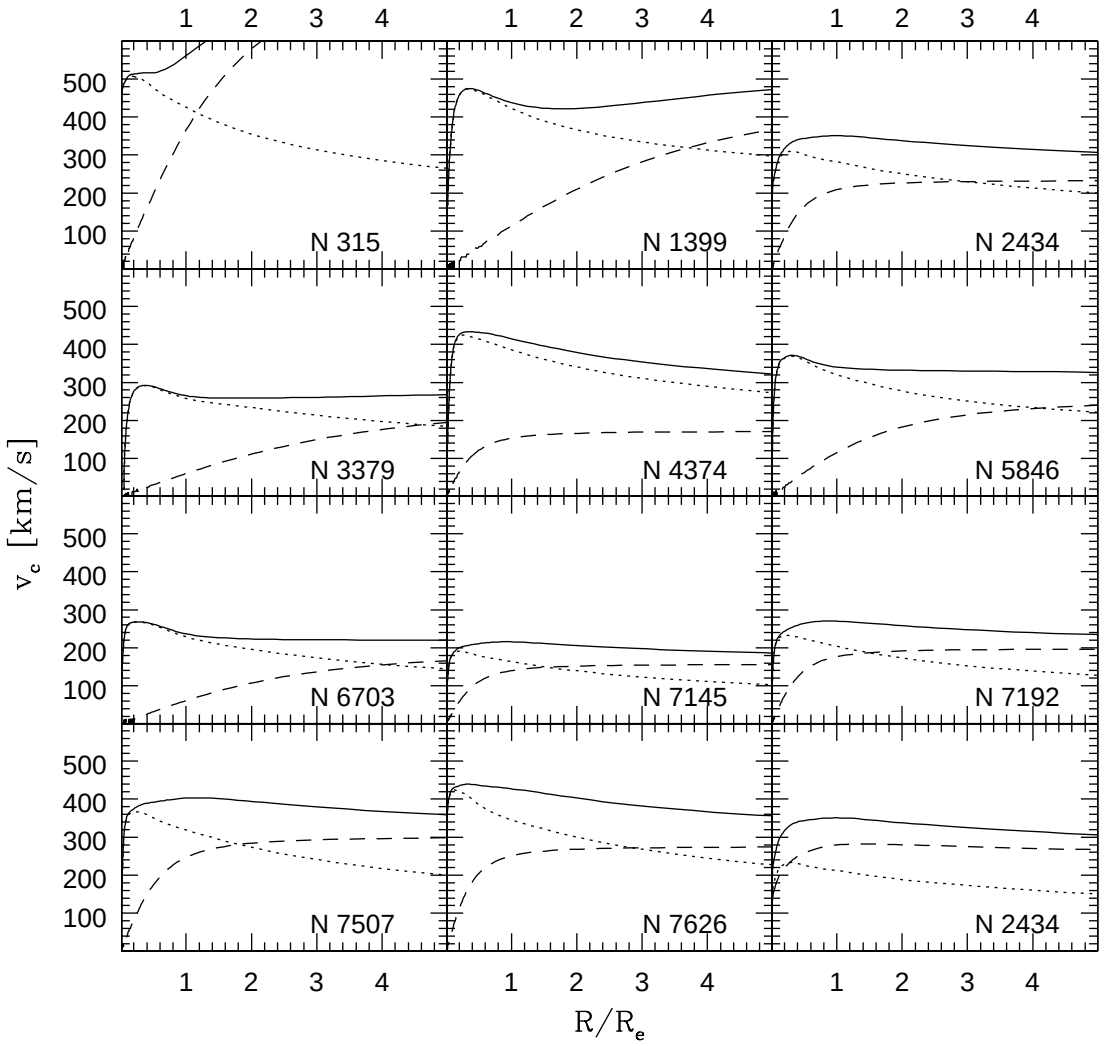

FIG. 17.—Total circular velocity curves (*solid lines*), and contributions of the luminous matter (*dotted lines*) and the dark halo (*dashed lines*). Note that the curves are extrapolated to $5R_e$.

of 4 below the Bell & de Jong (2000) and McGaugh et al. (2000) lines in Figure 9 (at $\log v_c^{\max} = 2.55$).

In a recent study, Loewenstein & White (1999) considered the implications of the observed X-ray temperature–velocity dispersion relation for the mass distribution and dark halos in elliptical galaxies. They found that the total (luminous plus dark) M/L_V at $6R_e$ is nearly independent of galaxy luminosity, with value $M/L_V(6R_e) \simeq 25h_{80}\, M_\odot/L_{\odot,V}$, so that the ratio of dark to luminous matter decreases with luminosity. Their $M/L(6R_e)$ converted to the B band and rescaled to h_{65} is consistent with the $M/L_B(6R_e)$ predicted by our models for $L_B \gtrsim L_*$ galaxies, while for our fainter galaxies the dynamical models predict ~ 0.2 dex lower mass per luminosity than given by Loewenstein & White (1999), in all cases, however, extrapolating the models beyond the radial range of the kinematic data. The dark matter mass fraction within R_e found from the X-ray analysis ($\gtrsim 20\%$) is in good agreement with our result quoted above.

5.3. *Dark Halo Parameters for Ellipticals*

In this section we investigate scaling laws for the halo densities and halo core radii of elliptical galaxies based on the "minimum halo models" of K + 2000. We also compare the inferred halo properties with the dark matter halos in spiral galaxies.

Figure 18 shows, as a function of galaxy luminosity, the effective radius R_e, the halo core radius $r_{c,h}$, the halo velocity v_h, core density ρ_h, and central phase-space density f_h, for the respective "best" models of K + 2000. All these correlate with luminosity, but the tightest correlation is that between the effective radius and the luminosity (one of the projections of the FP).

We note that for many of the galaxies in Figure 18 a constant M/L_B model with only luminous mass is within the 95% confidence range of the K + 2000 models. For these galaxies the halo radii, circular velocities, and densities have therefore large uncertainties in a logarithmic plot like Figure 18. However, in cases where X-ray data or planetary or globular cluster velocities were available, the "best" models of K + 2000 matched the independent mass estimates from these outer data very well, while the constant M/L models were usually inconsistent with these data. For seven of the sample galaxies, a constant M/L model was found inconsistent with the kinematic data (K + 2000). For these galaxies we have estimated 95% confidence bounds on the halo parameters from χ^2 contour plots and plotted them as error bars in Figure 18. In a few of these cases only the

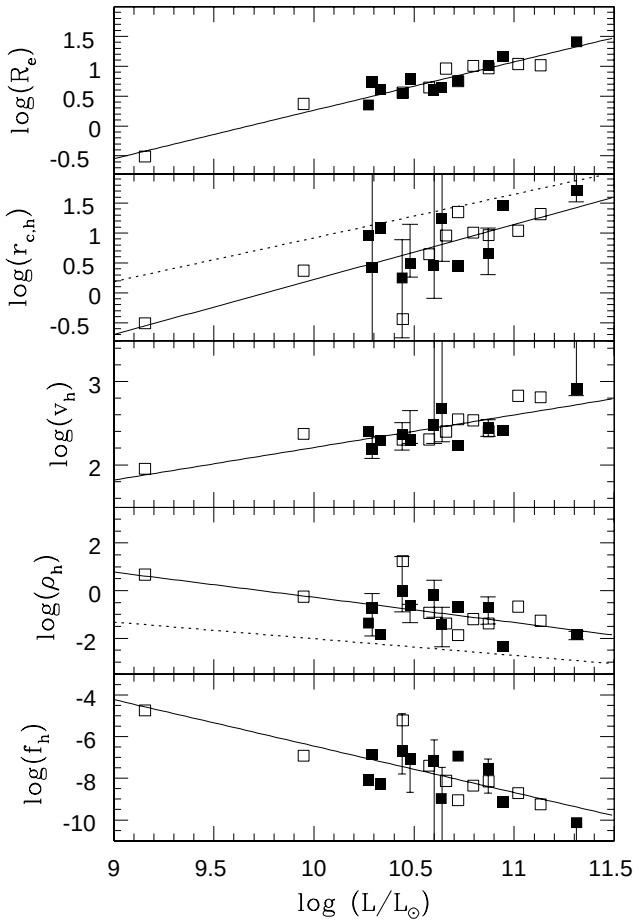

FIG. 18.—From top to bottom: effective radius in kpc vs. total luminosity in solar units; halo core radius in kpc; halo velocity in km s^{-1}; central halo density in $M_\odot$ pc^{-3}; and central halo phase-space density in $M_\odot$ pc^{-3} (km s^{-1})$^{-3}$, all referring to the "best" models selected by K + 2000 from the middle of the respective confidence range for all sample galaxies. Symbols are as in Fig. 5. The solid lines show the least-squares fits. Dotted lines show the corresponding relations for spiral galaxies given in the text.

halo density is well determined. Within the considerable uncertainties, the "error bars" are consistent with the scatter of the points. Note that some of the galaxies with the best evidence for dark halos (NGC 2434, 7507, 7626) are among the smallest halo core radii and largest halo density points with respect to the mean fit lines in Figure 18. By using the mean scaling relations from all the "best" halo models of K + 2000 for the subsequent discussion, we have therefore not biased the normalizations of the best-fit lines, while the best-fit slopes are much better determined.

Figure 18 shows that, in the mean, more luminous galaxies have larger halo core radii, with a slope similar to the log (R_e)–log (L) relation. They also have larger halo circular velocities, and lower central densities and phase-space densities. As predicted by hierarchical models less massive objects are denser. The least-squares fits shown in Figure 18 correspond to the following scaling laws:

$$R_e = 11.8 L_{11}^{0.81} h_{0.65}^{-1} \text{ kpc} , \quad (5)$$

$$r_{c,h} = 13.8 L_{11}^{0.92} h_{0.65}^{-1} \text{ kpc} , \quad (6)$$

$$v_h = 397 L_{11}^{0.39} \text{ km s}^{-1} , \quad (7)$$

$$\rho_h = 0.046 L_{11}^{-1.06} h_{0.65}^{2} \, M_\odot/\text{ pc}^3 , \quad (8)$$

$$f_h = 2.0 \times 10^{-9} L_{11}^{-2.23} h_{0.65}^{2} \, M_\odot/\text{pc}^3/(\text{km s}^{-1})^3 , \quad (9)$$

where $L_{11} = L_B/10^{11} h_{0.65}^{-2} L_{\odot,B}$,

$$\rho_h = \frac{3}{4\pi G} \frac{v_h^2}{r_{c,h}^2} \quad (10)$$

for the employed halo models (see eqs. [2]–[4] in Gerhard et al. 1998), and the central phase-space density is defined by

$$f_h \equiv 2^{3/2} \rho_h / v_h^3 . \quad (11)$$

Equations (5) and (6) result in a ratio of R_e and halo core radius that is approximately constant,

$$r_{c,h}/R_e = 1.2 L_{11}^{0.11} . \quad (12)$$

Also, from the results of § 3.5 and equations (5) and (10) one sees that the ratio of luminous mass density $(M/L_B)L_B/R_e^3$ and dark halo density has little luminosity dependence in the mean, although the scatter is large; the density ratio varies between $10^{\sim(0.5-2)}$.

The dotted lines in Figure 18 show the scaling relations for spiral galaxies from Persic, Salucci & Stel (1996, hereafter PSS), which are based on the same (minimum) halo models. The relation for spiral galaxy halo central densities as given by PSS and rescaled to the distance scale used here becomes

$$\rho_h^S = 0.0019 L_{11}^{-0.7} h_{0.65}^{2} \, M_\odot \text{ pc}^{-3} . \quad (13)$$

For luminosities around $L_B \simeq 10^{11} L_{B,\odot} \simeq 3L_*$, elliptical galaxy halos are therefore about 25 times denser than spiral galaxy halos of the same L_B, assuming maximum stellar mass in both cases. This result agrees well with the work of Bertola et al. (1993), who used extended H I disks around a few elliptical galaxies to constrain their halo mass distributions. Most of the factor 25 can be traced back to the fact that the CVCs of both spirals and ellipticals are approximately flat and that for an elliptical galaxy profile, the maximum circular velocity occurs at significantly smaller radius in units of R_e than for an exponential disk. There is an additional factor ~ 2 because of the larger M/L_B of ellipticals at given L_B.

According to PSS, the halo core radii of spiral galaxies also scale with luminosity when expressed in units of the optical radius. We can compare their relation to the case of elliptical galaxies as follows: Fitting the parameters R_e and L for ~ 200 spiral galaxies from the RC3, as given by Burstein et al. (1997), results in the least-squares fit line (rescaled to $H_0 = 65$ km s^{-1} Mpc^{-1})

$$R_e^S = 9.0 L_{11}^{0.53} h_{65}^{-1} \text{ kpc} . \quad (14)$$

This is somewhat shallower than the corresponding relation for elliptical galaxies, equation (5), but the R_e-values of spirals and ellipticals are very similar around $L = L_*$. Next, we use $R_{\rm opt}^S \equiv 3.2 R_D = 1.9 R_{1/2}^S$, where $R_{\rm opt}^S$, R_D, and $R_{1/2}^S$ are the optical, scale, and half-mass radius for an exponential disk, and we assume a mean $R_e^S = 1.2 R_D$ for the distribution between face-on and edge-on. From the relation given by PSS we then obtain

$$r_{c,h}^S/R_e^S = 5.0 L_{11}^{0.2} \quad (15)$$

and hence

$$r_{c,h}^S = 45 L_{11}^{0.73} h_{0.65}^{-1} \text{ kpc} . \quad (16)$$

Comparing these relations with equations (12) and (6), one sees that the minimum halos of spiral galaxies of the same L_B and R_e have about 4 times larger halo core radii than are inferred for elliptical galaxies from our dynamical analysis, and that the ratio is only slightly smaller at given L_B if the mean R_e^S (eq. [16]) is used. In view of the uncertainties in the transformations, the slopes in these relations appear consistent with each other.

Because of the luminosity offset in the TF relation, it may be more appropriate to compare elliptical and spiral galaxy halos at the same baryonic mass or circular velocity than at the same luminosity. Because this would mean comparing an elliptical galaxy with a spiral of *higher* luminosity, and because of the luminosity dependences in the spiral galaxy relations equations (16) and (13), this will *increase* the differences found above. Using $v_c^{\max}$ for the comparison as in Figure 7, the density ratio ρ_h/ρ_h^S thus increases by a factor of ~ 2. This may be an overestimate, however, as the inferred asymptotic halo velocities v_h are formally lower than $v_c^{\max}$ (by ~ 0.1 dex, compare eqs. [4] and [7]). We note here that the v_h-value for L_B^* predicted by equation (7), 253 km s^{-1}, is in agreement with the galaxy-galaxy lensing result of Wilson et al. (2000) at radii ~ 100 kpc, but emphasize that in our models v_h is much more uncertain than $v_c^{\max}$. Making the comparison at constant baryonic mass would increase the density ratio by a factor less than 1.6, from Figure 9 and equation (13). Thus, we conclude conservatively that the halos of elliptical galaxies are *at least* 25 times denser than the halos of spiral galaxies of similar baryonic mass or circular velocity.

These results also suggest that the phase-space densities for the minimum halos of elliptical galaxies are higher than for those of spiral galaxies of similar baryonic mass. From the TF relation spiral galaxies at given L_B have circular velocities about 0.2 dex lower than the $v_c^{\max}$ of elliptical galaxies, but perhaps only 0.1 dex lower than the v_h-values used in equations (7) and (9). This is not sufficient to compensate their lower densities. Higher phase-space densities would rule out stronger adiabatic contraction as the explanation for the denser halos in ellipticals. Recall also the similar R_e of ellipticals and spirals of the same L_B. The argument could be circumvented if spiral galaxies had submaximal disks and cuspy halos and their halo densities had been underestimated significantly by the PSS models. However, note that both in the Milky Way (Gerhard 1999) and in barred galaxies (Debattista & Sellwood 1998; Weiner et al. 2001), where independent dynamical constraints on the luminous mass are available, the galactic disks are near maximal, and that the recent stellar population models of Bell & de Jong (2001) suggest that high-surface brightness spirals are generally close to maximal disks.

One possible explanation for the much larger densities and probably phase-space densities of elliptical galaxy halos might be that some of the dark matter inferred in the inner regions of elliptical galaxies is baryonic. The evidence for large M/L ratios in ellipticals at large radii, of order 100, from both X-ray (e.g., Matsushita et al. 1998) and weak lensing data (Griffiths et al. 1998; Wilson et al. 2000), together with the lack of microlensing toward the LMC in the Milky Way (Alcock et al. 2000), does however not make this an attractive explanation for galactic halos in their entirety; a separate inner baryonic dark matter component would be needed.

An alternative possibility is that most elliptical galaxies formed at high redshift from progenitors with higher densities than seen in present-day spiral galaxies. If halo core densities are proportional to virial densities, which in turn depend on the density of the universe at the time of collapse, then the result above implies that elliptical galaxy halos have collapsed at redshifts $z_E \gtrsim 25^{1/3}(1 + z_S) - 1$, i.e., $z_E \gtrsim 5$ if the halos of spiral galaxies of similar luminosity formed at redshifts $z_S \gtrsim 1$. Thus, our result may indicate that giant elliptical galaxies are old, consistent with evidence from the fundamental plane (van Dokkum & Franx 1996; van Dokkum et al. 1998; Bender et al. 1998) and line-strength indices (Bender, Ziegler, & Bruzual 1996). Unfortunately, while this argument is plausible, it is not conclusive until the relation between the shallow central halo profiles inferred from observations and the cuspy halos predicted from hierarchical collapse of dark matter (NFW) is understood. Moreover, it would appear to be at odds with the observation of substantial merging in a moderate $z = 0.83$ cluster (van Dokkum et al. 1999), unless the progenitors had unusually high halo densities also, and also with the expectation that some elliptical galaxies should have formed recently from mergers of normal spiral galaxies (e.g., Schweizer 1998).

The plot of halo core radius against luminosity displays considerably larger scatter for both subsamples than the plot of R_e versus L and consequently also the inferred halo density shows considerable scatter at a given luminosity. What is the origin of this increased scatter? First, it is possible that modeling uncertainties contribute to the larger scatter in the derived $r_{c,h}$. However, we do not think that this can be the whole explanation. The three galaxies at the upper boundary of the points in the $r_{c,h}$-L-plot which have the best kinematic data for their kind, NGC 1399, NGC 3379, and NGC 6703, all have $\log (r_{ch}/R_e) = (0.5{:}0.6)$ and show evidence for small if any amount of dark matter within the modeled range. On the other hand, the best-determined galaxies near the lower boundary with the best evidence for additional dark matter, NGC 2434, 7507, 7626, have $\log (r_{ch}/R_e) = (-0.15{:} -0.35)$. Figure 17 shows that the two groups have significantly different CVC shapes *for the visible component only*: for the first group the visible CVC is almost coincident with the dynamically inferred total CVC to $1R_e$, whereas for the second group there are significant mass discrepancies already at $1R_e$. Thus, elliptical galaxies at fixed L_B appear to have a range of luminous matter CVCs and hence dark matter CVCs, even though the total CV rotation curves are fairly similar. Also, while the most rapidly rotating galaxies in the sample, for which we would expect the largest systematic errors in the modeling, have predominantly positive residuals with respect to the least-squares line, the nonrotating galaxies populate the entire distribution of residuals including the extremes. Thus, we believe that most of the scatter in the inferred $\log (r_{ch}/R_e)$ is not due to modeling effects, but reflects physical differences between the sample galaxies.

Could the amount of dark mass in the centers of preferentially those galaxies with apparently large r_{ch} have been underestimated with our minimum halo models? Then we would expect that the derived central M/L_B-values of these galaxies should be systematically high for their luminosity, i.e., we would expect a correlation of positive residuals from the M/L_B-L relation in Figure 13 with positive residuals in r_{ch}-L. However, the M/L_B residuals for galaxies with large

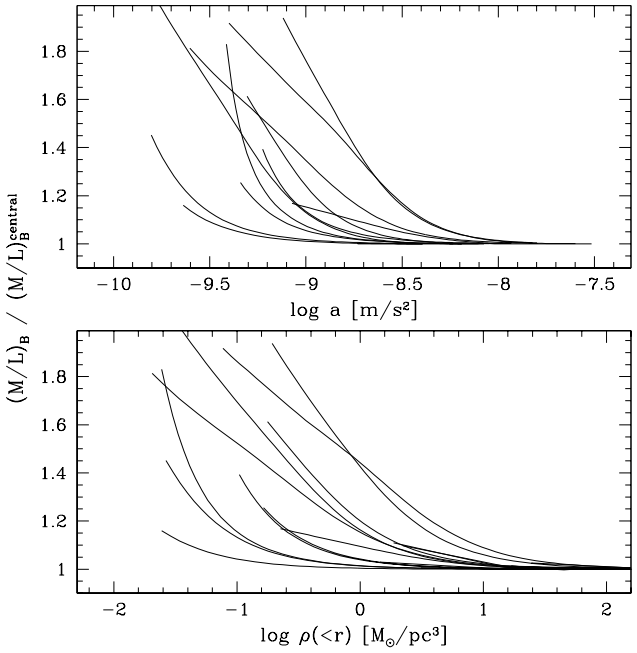

FIG. 19.—*Top*: *B*-band M/L_B, normalized by the central M/L_B, vs. the gravitational acceleration v^2/r for all galaxies from the EK subsample. The "bending upward" occurs at accelerations $a \sim 10^{-9}$ m s^{-2}, a factor of 10 higher than typical in spiral galaxies. *Bottom*: Normalized M/L_B vs. mean interior density.

and small halo core radii for their luminosities do not show a systematic difference in the present sample.

Thus, we believe the most likely explanation for the larger scatter in r_{ch} is that galaxies of similar luminosity have different dark matter core radii and central densities determined by the particulars of the merging process in which they were made. In this case the scatter in inferred halo density (an order of magnitude or more) should perhaps reflect mainly the halo densities of the progenitors at the time of formation, with the highest (lowest) densities corresponding to the earliest (latest) mergers. We have attempted to test this by plotting the minimum halo densities from Figure 18 versus the population ages of § 4, but no convincing correlation is seen in the present data.

Figure 19 finally shows mass-to-light ratios M/L_B normalized by the central value, as a function of acceleration $a = v_c^2(r)/r$ and mean interior density $\rho(<r) \equiv 3v_c^2(r)/4\pi G r^2$, for all galaxies in the EK subsample with extended data. The estimated uncertainty in a from that in v_c and distance is of order 50%. Figure 19 shows that the "bending upward" which indicates the onset of dark matter takes place at systematically higher accelerations a than in spiral galaxies (McGaugh 1999), by about 1 order of magnitude, which is a consequence of the higher halo mass densities in elliptical galaxies. This suggests that the acceleration scale found in spiral galaxies is not universal as required by the modified gravity theory MOND (Milgrom 1983), i.e., that in elliptical galaxies an additional gradient in M/L would be required besides MOND.

6. CONCLUSIONS

Based on a uniform dynamical analysis of photometric and line-profile shape data for 21 mostly luminous, slowly rotating, and nearly round (17 E0/E1 and four E2) elliptical galaxies by Kronawitter et al. (2000), we have investigated the dynamical family relations and dark halo properties of ellipticals. Our main results are as follows:

1. The circular velocity curves (CVCs) of elliptical galaxies are flat to within $\simeq 10\%$ for $R \gtrsim 0.2R_e$ to at least $R \gtrsim 2R_e$, independent of luminosity. This argues against strong luminosity segregation in the dark halo potential.
2. Most ellipticals are moderately radially anisotropic, with average $\beta \simeq 0$–0.35, again independent of luminosity.
3. The dynamical structure of ellipticals is surprisingly uniform. The maximum circular velocity is accurately predicted by a suitably defined central velocity dispersion.
4. Elliptical galaxies follow a Tully-Fisher (TF) relation with marginally shallower slope than spiral galaxies. At given circular velocity, they are about 1 mag fainter in B and about 0.6 mag in R, and appear to have slightly lower baryonic mass than spirals, even for the maximum M/L_B allowed by the kinematics.
5. The residuals from the TF and fundamental plane (FP) relations do not correlate with dynamical anisotropy β.
6. The luminosity dependence of M/L indicated by the tilt of the FP corresponds to a real dependence of dynamical M/L on L. The tilt of the FP is therefore not due to deviations from homology or a variation of dynamical anisotropy with L, although the slope of M/L versus L could still be influenced by photometric nonhomology. The tilt can also not be due to an increasing dark matter fraction with L, unless (i) the most luminous ellipticals have a factor >3 less baryonic mass than spiral galaxies of the same circular velocity, (ii) the range of IMF is larger than currently discussed, and (iii) the IMF or some other population parameter varies systematically along the luminosity sequence such as to undo the increase of M/L expected from simple stellar population models for more metal-rich luminous galaxies. This seems highly unlikely.
7. The tilt of the FP is therefore best explained as a stellar population effect. Population models show that the values and the change with L_B of the maximal dynamical M/L_B-values are consistent with the stellar population M/L_B-values based on published metallicities and ages within the uncertainties of IMF and distance scale. The main driver is therefore probably metallicity, and a secondary population effect is needed to explain the K-band tilt.
8. The population models show that we would have overestimated the luminous masses by as much as a factor ≈ 2 only if (i) the flattest IMFs at low stellar masses discussed for the Milky Way are applicable to our elliptical galaxies, and simultaneously (ii) a short distance scale ($H_0 \simeq 80$ km s^{-1} Mpc^{-1}) turns out to be correct. For lower values of H_0 and/or the other IMFs investigated in § 4 the difference is smaller. Together with (4) this makes it likely that elliptical galaxies have indeed nearly maximal M/L_B ratios (minimal halos).
9. Despite the uniformly flat CVCs, there is a spread in the ratio of the CVCs from luminous and dark matter, i.e., in the radial variations of cumulative mass-to-light ratio. The sample includes galaxies with no indication for dark matter within $2R_e$, and others where the best dynamical models result in local M/L_B-values of 20–30 at $2R_e$. As in spiral galaxies, the combined rotation curve of the luminous and dark matter is flatter than those for the individual components ("conspiracy").

10. In models with maximum stellar mass, the dark matter contributes $\sim 10\%$–40% of the mass within R_e. Our flat rotation curve models, when extrapolated beyond the range of kinematic data, predict equal interior mass of dark and luminous matter at ~ 2–$4R_e$, consistent with results from the X-ray temperature–velocity relation.

11. Even in these maximum stellar mass models, the halo core densities and phase-space densities are at least ~ 25 times larger and the halo core radii ~ 4 times smaller than in spiral galaxies of the same circular velocity. Correspondingly, the increase in M/L sets in at ~ 10 times larger acceleration than in spirals. This could imply that elliptical galaxy halos collapsed at high redshifts or that some of the dark matter in ellipticals might be baryonic.

We thank D. Forbes for providing ages and metallicities for some of our sample galaxies in electronic form, C. Maraston for help with her stellar population models, and M. Samland for assistance with IDL. We acknowledge helpful discussions with H.-W. Rix and G. A. Tammann. O. G. and A. K. were supported by grant 20-56888.99 from the Schweizerischer Nationalfonds, R. P. S. and R. B. acknowledge the support by DFG grant SFB 375.

REFERENCES

Alcock, C., et al. 2000, ApJ, 542, 281
Athanassoula, E., Bosma, A., & Papaioannou, S. 1987, A&A, 179, 23
Bell, E. F., & de Jong, R. S. 2001, ApJ, in press (astro-ph/0011493)
Bender, R., Saglia, R. P., & Gerhard, O. 1994, MNRAS, 269, 785
Bender, R., Saglia, R. P., Ziegler, B., Belloni, P., Greggio, L., Hopp, U., & Bruzual, G. 1998, ApJ, 493, 529
Bender, R., Ziegler, B., & Bruzual, G. 1996, ApJ, 463, L51
Bertola, F., Pizzella, A., Persic, M., & Salucci, P. 1993, ApJ, 416, L45
Burstein, D., Bender, R., Faber, S. M., & Nolthenius, R. 1997, AJ, 114, 1365
Cretton, N., Rix, H.-W., & de Zeeuw, T. 2000, ApJ, 536, 319
Courteau, S., & Rix, H.-W. 1999, ApJ, 513, 561
de Vaucouleurs, G., de Vaucouleurs, A., Corwin, H. G., Jr., Buta, R. J., Paturel, G., & Fouque, P. 1991, Third Reference Catalogue of Bright Galaxies, Version 3.9 (New York: Springer) (RC3)
Debattista, V., & Sellwood, J. A. 1998, ApJ, 493, L5
Djorgovski, S., & Davis, M. 1987, ApJ, 313, 59
Dressler, A., Lynden-Bell, D., Burstein, D., Davies, R. L., Faber, S. M., Terlevich, R. J., & Wegner, G. 1987, ApJ, 313, 42
Faber, S. M., Dressler, A., Davies, R. L., Burstein, D., Lynden-Bell, D., Terlevich, R. J., & Wegner, G. 1987, in Nearly Normal Galaxies, from the Planck Time to the Present, ed. S. M. Faber (New York: Springer), 175
Faber, S., & Jackson, R. E. 1976, ApJ, 204, 668
Faber, S., Wegner, G., Burstein, D., Davies, R. L., Dressler, A., Lynden-Bell, D., & Terlevich, R. 1989, ApJS, 69, 763
Federspiel, M., Tammann, G. A., & Sandage, A. 1998, ApJ, 495, 115
Forbes, D. A., & Ponman, T. J. 1999, MNRAS, 309, 623
Forbes, D. A., Ponman, T. J., & Brown, R. J. 1998, ApJ, 508, L43
Forman, W., Jones, C., & Tucker, W. 1985, ApJ, 293, 102
Fukugita, M., & Turner, E. L. 1991, MNRAS, 253, 99
Gebhardt, K., et al. 2000, AJ, 119, 1157
Gerhard, O. E. 1999, in ASP Conf. Ser. 182, Galaxy Dynamics, ed. D. Merritt, M. Valluri, & J. Sellwood (San Francisco: ASP), 307
Gerhard, O. E., Jeske, G., Saglia, R. P., & Bender, R. 1998, MNRAS, 295, 197
Gould, A., Bahcall, J. N., & Flynn, C. 1997, ApJ, 482, 913 (GBF)
Graham, A., & Colless, M. M. 1997, MNRAS, 287, 221
Griffiths, R. E., Casertano, S., Im, M., & Ratnatunga, K. U. 1998, MNRAS, 282, 1159
Holtzman, J. A., et al. 1998, AJ, 115, 1946
Jørgensen, I., Franx, M., & Kjærgard, P. 1996, MNRAS, 280, 167
Kaeppeli, A. 1999, diploma thesis, Univ. Basel
Keeton, C. R., Kochanek, C. S., & Falco, E. E. 1998, ApJ, 509, 561
Kobayashi, C., & Arimoto, N. 1999, ApJ, 527, 573
Kochanek, C. S. 1995, ApJ, 445, 559
Kronawitter, A., Saglia, R. P., Gerhard, O. E., & Bender, R. 2000, A&AS, 144, 53 (K+2000)
Kroupa, P. 2000, MNRAS, in press (astro-ph/0009005)
Loewenstein, M., & White, R. E. 1999, ApJ, 518, 50
Maraston, C. 1998, MNRAS, 300, 872
———. 1999, in ASP Conf. Ser. 163, Star Formation in Early-type Galaxies, ed. J. Cepa & P. Carral (San Francisco: ASP), 28
Maraston, C., & Thomas, D. 2000, ApJ, 541, 126
Matsushita, K., Makishima, K., Ikebe, Y., Rokutanda, E., Yamasaki, N. Y., & Ohashi, T. 1998, ApJ, 499, L13
Matthias, M., & Gerhard, O. E. 1999, MNRAS, 310, 879
McGaugh, S. 1999, in ASP Conf. Ser. 182, Galaxy Dynamics, ed. D. Merritt, M. Valluri, & J. Sellwood (San Francisco: ASP), 528
McGaugh, S., Schombert, J. M., Bothun, G. D., & de Blok, W. J. G. 2000, ApJ, 533, L99
Mehlert, D., Saglia, R. P. Bender, R., & Wegner, G. 1998, A&A, 332, 33
Milgrom, M. 1983, ApJ, 270, 365
Mushotzky, R. F., Loewenstein, M., Awaki, H., Makishima, K., Matsushita, K., & Matsumoto, H. 1994, ApJ, 436, L79
Navarro, J., Frenk, C. S., & White, S. D. M. 1996, ApJ, 462, 563 (NFW)
Neistein, E., Maoz, D., Rix, H.-W., & Tonry, J. L. 1999, AJ, 117, 2666
Pahre, M. A., Djorgovski, S. G., & de Carvalho, R. R. 1998, AJ, 116, 1591
Persic, M., Salucci, P., & Stel, F. 1996, MNRAS, 281, 27 (erratum 283, 1102) (PSS)
Press, W. H., Teukolsky, S. A., Vetterling, W. T., & Flannery, B. P. 1992, Numerical Recipes in C (2d ed.; Cambridge: Cambridge Univ. Press)
Rix, H.-W., de Zeeuw, P. T., Cretton, N., van der Marel, R., & Carollo, C. M. 1997, ApJ, 488, 702
Rubin, V. C., Waterman, A. H., & Kenney, J. D. 1999, ApJ, 118, 236
Saglia, R. P., et al. 1997a, MNRAS, 292, 499
Saglia, R. P., et al. 1997b, ApJS, 109, 79
Saglia, R. P., Kronawitter, A., Gerhard, O. E., & Bender, R. 2000a, AJ, 119, 153
Saglia, R. P., Maraston, C., Greggio, L., Bender, R., & Ziegler, B. 2000b, A&A, 360, 911
Sakai, S., et al. 2000, ApJ, 529, 698
Salucci, P., & Persic, M. 1999, A&A, 351, 442
Sarazin, C. L. 1997, in ASP Conf. Ser. 116, The Nature of Elliptical Galaxies, ed. M. Arnaboldi, G. S. da Costa, & P. Saha (San Francisco: ASP), 375
Schweizer, F. 1998, in Galaxies: Interactions and Induced Star Formation, ed. R. C. Kennicutt, F. Schweizer, J. E. Barnes, D. Friedli, L. Martinet, & D. Pfenniger (Berlin: Springer), 105
Terlevich, A., & Forbes, D. A. 2000, MNRAS, submitted
Trager, S. C., Faber, S. M., Worthey, G., & Gonzaléz, J. J. 2000a, AJ, 119, 1645
———. 2000b, AJ, 120, 165
Tonry, J. L., Blakeslee, J. P., Ajhar, E. A., & Dressler, A. 1997, ApJ, 475, 399
Tully, R. B., & Fisher, J. R. 1977, A&A, 54, 661 (TF)
van Dokkum, P. G., & Franx, M. 1996, MNRAS, 281, 985
van Dokkum, P. G., Franx, M., Fabricant, D., Kelson, D. D., & Illingworth, G. 1999, ApJ, 520, L95
van Dokkum, P. G., Franx, M., Kelson, D. D., & Illingworth, G. 1998, ApJ, 504, L17
Weiner, B. J., Sellwood, J. A., & Williams, T. B. 2001, ApJ, 546, 916
Wilson, G., Kaiser, N., Luppino, G. A., & Cowie, L. L. 2000, preprint (astro-ph/0008504)
Worthey, G. 1994, ApJS, 95, 107